56. Hansma, H.; Weisenhorm, A.; Edmundson, A.; Gaub, H.; Hansma, P., *Clin. Chem.* **37**, 1497 (1991).
57. Gardner, C. E.; Macpherson, J. V., *Anal. Chem.* **74**, 576A (2002).
58. Jones, V.; Kenseth, J.; Porter, M. D.; Mosher, C. L.; Henderson, E., *Anal. Chem.* **70**, 1233 (1998).
59. Demers, L. M.; Ginger, D.; Park, S.; Li, Z.; Chung, S.; Mirkin, C. A., *Science* **296**, 1836 (2002).
60. Liu, W.; Montana, V.; Chapman, E. R.; Mohideen, U.; Parpura, V., *Proc. Natl. Acad. Sci. USA* **100**, 13621 (2003).
61. Wickramaasinghe, H., *Scientific Am.* **98** (Oct. 1989).
62. Engstrom, R.; Pharr, C., *Anal. Chem.* **61**, 1099A (1989).
63. Bard, A. J.; Denuault, G.; Lee, C.; Mandler, D.; Wipf, D., *Acc. Chem. Res.* **23**, 357 (1990).
64. Mirkin, M. V., *Anal. Chem.* **68**, 177A (1996).
65. Arca, M.; Bard, A. J.; Horrocks, B.; Richards, T.; Treichel, D., *Analyst* **119**, 719 (1994).
66. Liu, H.; Fan, F.; Lin, C.; Bard, A. J., *J. Am. Chem. Soc.* **108**, 3838 (1986).
67. Kwak, J.; Bard, A. J., *Anal. Chem.* **61**, 1794 (1989).
68. Fan, F.; Kwak, J.; Bard, A. J., *J. Am. Chem. Soc.* **118**, 9669 (1996).
69. Wang, J.; Wu, L.; Li, R., *J. Electroanal. Chem.* **272**, 285 (1989).
70. Pierce, D.; Unwin, P.; Bard, A. J., *Anal. Chem.* **64**, 1795 (1992).
71. Bath, B. D.; Scott, E. R.; Phipps, J. B.; White, J. S., *J. Pharm. Sci.* **89**, 1537 (2000).
72. Yasukawa, T.; Kaya, T.; Matsue, T., *Electroanalysis* **12**, 653 (2000).
73. Yamashita, K.; Takagi, M.; Uchida, K.; Kondo, H.; Takenak, S., *Analyst* **126**, 1210 (2001).
74. Horrocks, B.; Mirkin, M.; Pierce, D.; Bard, A. J.; Nagy, G.; Toth, K., *Anal. Chem.* **65**, 1304 (1993).
75. Wei, C.; Bard, A. J.; Nagy, G.; Toth, K., *Anal. Chem.* **67**, 1346 (1995).
76. Nowall, W.; Wipf, D.; Kuhr, W. G., *Anal. Chem.* **70**, 2601 (1998).
77. *Scanning Electrochemical Microscope*, CH Instruments, 1998.
78. Smith, J. P., *Anal. Chem.* **73**, 39A (2001).
79. Kranze, C.; Friedbacher, G.; Mizaikoff, B.; Lugstein, A.; Smoliner, J.; Bertagnolli, E., *Anal. Chem.* **73**, 2491 (2001).
80. Boldt, F.; Heinze, J.; Diez, M.; Peterson, J.; Börsch, M., *Anal. Chem.* **76**, 3473 (2004).
81. Basak, S.; Bose, C.; Rajeshwar, K., *Anal. Chem.* **64**, 1813 (1992).
82. Hillman, A. R.; Loveday, D.; Swann, M.; Bruckenstein, S.; Wildle, C. P., *Analyst* **117**, 1251 (1992).
83. Deakin, M.; Buttry, D., *Anal. Chem.* **61**, 1147A (1989).
84. Ward, M. D.; Buttry, D. A., *Science* **249**, 1000 (1990).
85. Cliffel, D.; Bard, A. J., *Anal. Chem.* **70**, 1993 (1998).
86. Tatsuma, T.; Watanabe, Y.; Oyama, N.; Kiakizaki, K.; Haba, M., *Anal. Chem.* **71**, 3632 (1999).
87. Park, S. M.; Yoo, J. S., *Anal. Chem.* **75**, 455A (2003).
88. Katz, E.; Willner, I., *Electroanalysis* **15**, 913 (2003).

3

CONTROLLED-POTENTIAL TECHNIQUES

The basis of all controlled-potential techniques is the measurement of the current response to an applied potential. A multitude of potential excitations (including a ramp, potential steps, pulse trains, a sine wave, and various combinations thereof) exists. The present chapter reviews those techniques that are widely used.

3.1 CHRONOAMPEROMETRY

Chronoamperometry involves stepping the potential of the working electrode from a value at which no faradaic reaction occurs to a potential at which the surface concentration of the electroactive species is effectively zero (Fig. 3.1a). A stationary working electrode and unstirred (quiescent) solution are used. The resulting current–time dependence is monitored. As mass transport under these conditions is solely by diffusion, the current–time curve reflects the change in the concentration gradient in the vicinity of the surface (recall Section 1.2). This involves a gradual expansion of the diffusion layer associated with the depletion of the reactant, and hence decreased slope of the concentration profile as time progresses (see Fig. 3.1b). Accordingly, the current (at a planar electrode) decays with time (Fig. 3.1c), as given by the *Cottrell equation*

Analytical Electrochemistry, Third Edition, by Joseph Wang

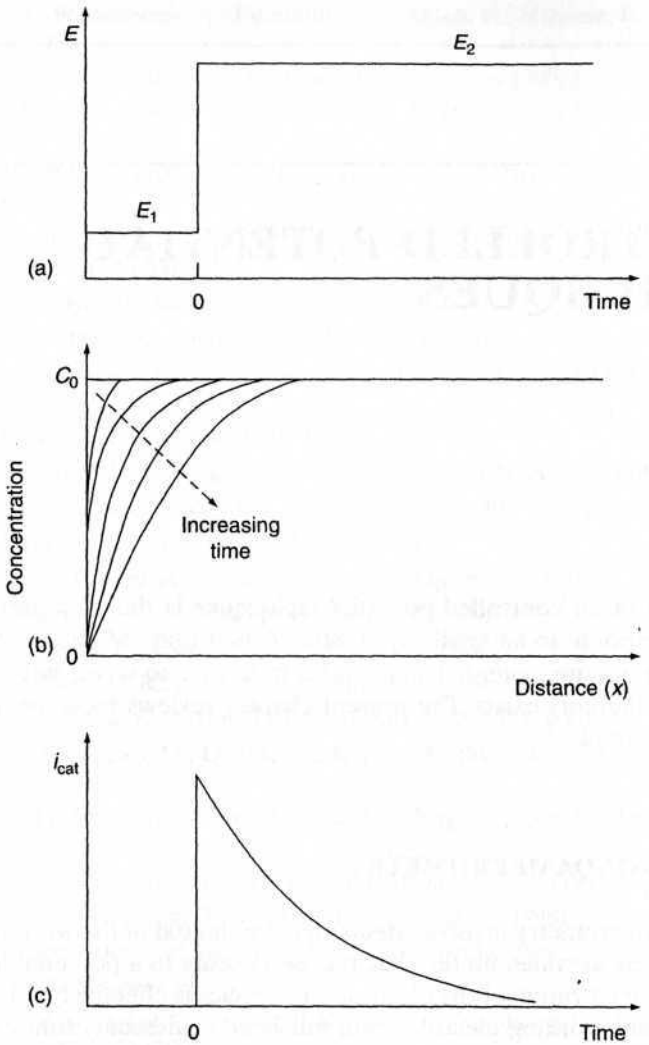

Figure 3.1 Chronoamperometric experiment: (a) potential–time waveform; (b) change in concentration profiles as time progresses; (c) the resulting current–time response.

$$i(t) = \frac{nFACD^{1/2}}{\pi^{1/2}t^{1/2}} = kt^{-1/2} \tag{3.1}$$

where n, F, A, C, D, and t are the number of electrons, Faraday's constant, the surface area, the concentration, the diffusion coefficient, and time, respectively. Such an $it^{1/2}$ constancy is often termed a "Cottrell behavior." Deviations from such behavior occur at long times (usually over 100 s) as a result of natural

convection effects, due to coupled chemical reactions, and when using non-planar electrodes or microelectrodes with high perimeter : area ratio (see Section 4.5.4). In the latter case, a time-independent current (proportional to the concentration) is obtained for $t > 0.1$ s, due to a large radial diffusion contribution. Similar considerations apply to spherical electrodes whose current response following potential step contains time-dependent and time-independent terms [Eq. (1.12)]. Recall also that for short values of t ($t < 50$ ms), the chronoamperometric signal contains an additional background contribution of the charging current [Eq. (1.49)]. This exponentially decaying charging current represents the main contribution to the response in the absence of an electroactive species.

Chronoamperometry is often used for measuring the diffusion coefficient of electroactive species or the surface area of the working electrode. Some analytical applications of chronoamperometry (e.g., in vivo bioanalysis) rely on pulsing of the potential of the working electrode repetitively at fixed time intervals. Some popular test strips for blood glucose (discussed in Chapter 6) involve potential-step measurements of an enzymatically liberated product (in connection with a preceding incubation reaction). Chronoamperometry can also be applied to the study of mechanisms of electrode processes. Particularly attractive for this task are reversal double-step chronoamperometric experiments (where the second step is used to probe the fate of a species generated in the first one).

The potential-step experiment can also be used to record the charge–time dependence. This is accomplished by integrating the current resulting from the potential step and adding corrections for the charge due to the double-layer charging (Q_{dl}) and reaction of the adsorbed species (Q_i):

$$Q = \frac{2nFACD^{1/2}t^{1/2}}{\pi^{1/2}} + Q_{dl} + Q_i \tag{3.2}$$

Such a charge measurement procedure, known as *chronocoulometry*, is particularly useful for measuring the quantity of adsorbed reactants (because of the ability to separate the charges produced by the adsorbed and solution species). A plot of the charge (Q) versus $t^{1/2}$, known as an *Anson plot*, yields an intercept at $t = 0$ that corresponds to the sum of Q_{dl} and Q_i (Fig. 3.2). The former can be estimated by subtracting the intercept obtained in an identical experiment carried out in the blank solution.

3.2 POLAROGRAPHY

Polarography is a subclass of voltammetry in which the working electrode is dropping mercury. Because of the special properties of this electrode, particularly its renewable surface and wide cathodic potential range (see Chapters 3–5 for details), polarography has been widely used for the determination of

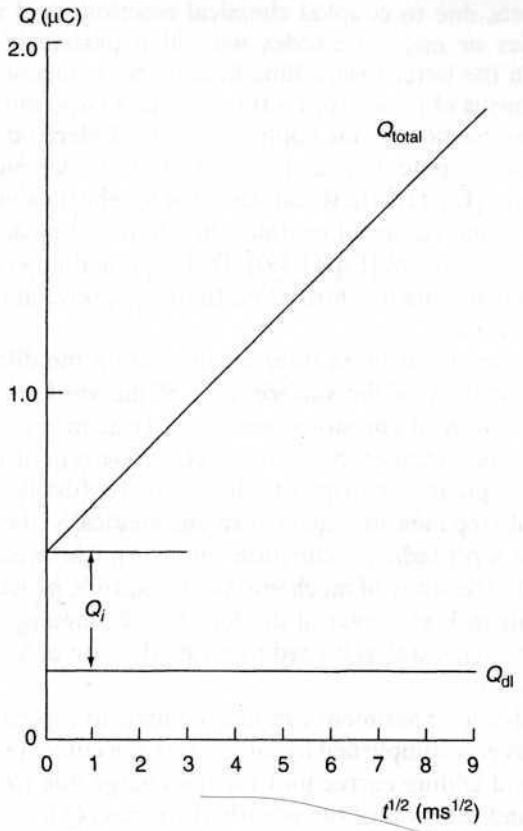

Figure 3.2 Chronocoulometric experiment: Anson plot of Q versus $t^{1/2}$.

many important reducible species. This classical technique was invented by J. Heyrovsky in Czechoslovakia in 1922, and had an enormous impact on the progress of electroanalysis (through many subsequent developments). Accordingly, Heyrovsky was awarded the 1959 Noble Prize in Chemistry.

The excitation signal used in conventional (DC) polarography is a linearly increasing potential ramp. For a reduction, the initial potential is selected to ensure that the reaction of interest does not take place. The potential is then scanned cathodically while the current is measured. Such current is proportional to the slope of the concentration–distance profile (see Section 1.2.1.2). At a sufficiently negative potential, reduction of the analyte commences, the concentration gradient increases, and the current rises rapidly to its limiting (diffusion-controlled) value. At this plateau, any analyte particle that arrives at the electrode surface instantaneously undergoes an electron transfer reaction, and the maximum rate of diffusion is achieved. The resulting polarographic wave is shown in Figure 3.3. The current oscillations reflect the growth and fall of the individual drops.

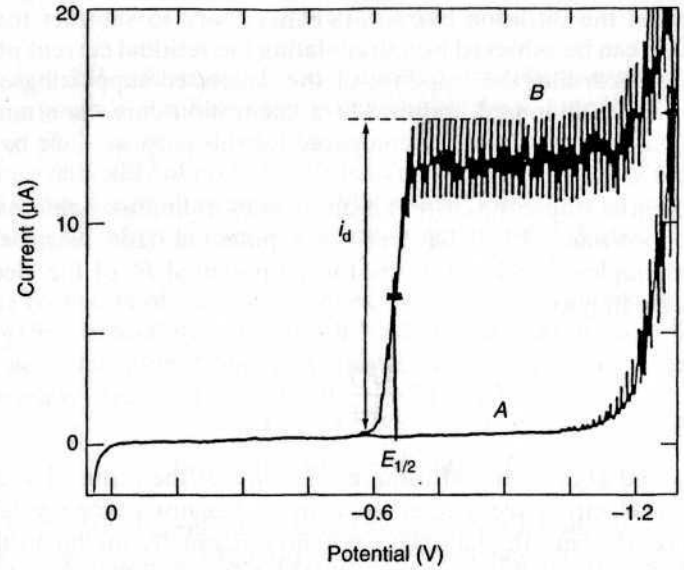

Figure 3.3 Polarograms for 1 M hydrochloric acid (A) and 4×10^{-4} M Cd^{2+} in 1 M hydrochloric acid (B); i_d represents the limiting current, while $E_{1/2}$ is the half-wave potential.

To derive the expression for the current response, one must account for the variation of the drop area with time

$$A = 4\pi\left(\frac{3mt}{4\pi d}\right)^{2/3} = 0.85(mt)^{2/3} \tag{3.3}$$

where t is the time and m and d are the mass flow rate and density of mercury, respectively. By substituting the surface area [from Eq. (3.3)] into the Cottrell equation [Eq. (3.1)], and replacing D by $7/3D$ (to account for the compression of the diffusion layer by the expanding drop), we can obtain the *Ilkovic equation* for the limiting diffusion current (1):

$$i_d = 708nD^{1/2}m^{2/3}t^{1/6}C \tag{3.4}$$

Here, i_d will have units of amperes (A), when D is in cm^2/s, m is in g/s, t is in seconds, and C is in mol/cm^3. This expression represents the current at the end of the drop life. The average current over the drop life is obtained by integrating the current of this time period:

$$i_{av} = 607nD^{1/2}m^{2/3}t^{1/6}C \tag{3.5}$$

To determine the diffusion current, it is necessary to subtract the residual current. This can be achieved by extrapolating the residual current prior to the wave or by recording the response of the deaerated supporting electrolyte (blank) solution. Standard addition or a calibration curve is often used for quantitation. Polarograms to be compared for this purpose must be recorded in the same way.

The potential where the current is one-half of its limiting value is called the *half-wave potential*, $E_{1/2}$. The half-wave potential (for electrochemically reversible couples) is related to the formal potential $E°$ of the electroactive species according to

$$E_{1/2} = E° + \frac{RT}{nF}\log(D_R/D_O)^{1/2} \tag{3.6}$$

where D_R and D_O are the diffusion coefficients of the reduced and oxidized forms of the electroactive species, respectively. Because of the similarity in the diffusion coefficients, the half-wave potential is usually similar to the formal potential. Thus, the half-wave potential, which is a characteristic of a particular species in a given supporting electrolyte solution, is independent of the concentration of that species. Therefore, by measuring the half-wave potential, one can identify the species responsible for an unknown polarographic wave. Typical half-wave potentials for several reducible organic functionalities, common in organic compounds, are given in Table 3.1. Compounds containing these functionalities are ideal candidates for polarographic measurements. (Additional oxidizable compounds can be measured using solid–electrode voltammetric protocols.) Since neutral compounds are involved, such organic polarographic reductions commonly involve hydrogen ions. Such reactions can be represented as

TABLE 3.1 Functional Groups Reducible at the DME

Class of Compounds	Functional	$E_{1/2}$ (V[a]) Group
Azo	—N=N—	–0.4
Carbon–carbon double bond[b]	—C=C—	–2.3
Carbon–carbon triple bond[b]	—C≡C—	–2.3
Carbonyl	>C=O	–2.2
Disulfide	S—S	–0.3
Nitro	NO_2	–0.9
Organic halides	C—X (X = Br, Cl, I)	–1.5
Quinone	C=O	–0.1

[a] Against the saturated calomel electrode at pH = 7.
[b] Conjugated with a similar bond or with an aromatic ring.

$$R + nH^+ + ne^- \rightleftharpoons RH_n \tag{3.7}$$

where R and RH_n are oxidized and reduced forms of the organic molecule. For such processes, the half-wave potential will be a function of pH (with a negative shift of about 59 mV/n for each unit increase in pH, due to decreasing availability of protons). Thus, in organic polarography, good buffering is vital for generating reproducible results. Reactions of organic compounds are also often slower and more complex than those for inorganic cations.

For the reduction of metal complexes, the half-wave potential is shifted to more negative potentials, reflecting the additional energy required for the complex decomposition. Consider the reversible reduction of a hypothetical metal complex, ML_p:

$$ML_p + ne^- + Hg \rightleftharpoons M(Hg) + pL \tag{3.8}$$

where L is the free ligand and p is the stoichiometric number. (The charges are omitted for simplicity.) The difference between the half-wave potential for the complexed and uncomplexed metal ion is given by (2)

$$(E_{1/2})_c - (E_{1/2})_{free} = \frac{RT}{nF}\ln K_d - \frac{RT}{nF}p\ln[L] + \frac{RT}{nF}\ln\left(\frac{D_{free}}{D_c}\right)^{1/2} \tag{3.9}$$

where K_d is the formation constant. The stoichiometric number can thus be computed from the slope of a plot $(E_{1/2})_c$ versus ln [L]. It is possible to exploit Eq. (3.9) to improve the resolution between two neighboring polarographic waves, based on a careful choice of the ligand and its concentration.

For reversible systems (with fast electron transfer kinetics), the shape of the polarographic wave can be described by the Heyrovsky–Ilkovic equation:

$$E = E_{1/2} + \frac{RT}{nF}\ln\left(\frac{i_d - i}{i}\right) \tag{3.10}$$

It follows from this equation that a plot of E versus log $[(i_d - i)/i]$ should yield a straight line with a slope of 0.059/n at 25°C. Such a plot offers a convenient method for the determination of n. In addition, the intercept of this line will be the half-wave potential. Another way to estimate n is to measure $(E_{3/4} - E_{1/4})$, which corresponds to 56.4/n mV for a reversible system ($E_{3/4}$ and $E_{1/4}$ are the potentials for which $i = 0.75i_d$ and $i = 0.25i_d$, respectively). It should be emphasized that many polarographic processes, especially those of organic compounds, are not reversible. For those that depart from reversibility, the wave is "drawn out," with the current not rising steeply, as is shown in Figure 3.3. The shape of the polarographic response for an irreversible reduction process is given by

$$E = E^\circ + \frac{RT}{\alpha n F} \ln\left[1.35 k_f \left(\frac{i_d - i}{i}\right)\left(\frac{t}{D}\right)^{1/2}\right] \tag{3.11}$$

where α is the transfer coefficient and k_f is the rate constant of the forward reaction.

In a few instances, the polarographic wave is accompanied by a large peak (where the current rises to a maximum before returning to the expected diffusion current plateau). Such an undesired peak, known as the *polarographic maximum*, is attributed to a hydrodynamic flow of the solution around the expanding mercury drop, can be suppressed by adding a small amount of a surface-active material (such as Triton X-100).

When the sample solution contains more than one reducible species, diffusion currents resulting from each of them are observed. The heights of the successive waves can be used to measure the individual analytes, provided there is a reasonable difference (>0.2 V) between the half-wave potentials. The baseline for measuring the limiting current of the second species is obtained by extrapolation of the limiting current of the first process. With a potential window of ~2 V, five to seven individual polarographic waves could be observed. Solution parameters, such as the pH or concentration of complexing agents, can be manipulated to deliberately shift the peak potential and hence to improve the resolution of two successive waves. Successive waves are also observed for samples containing a single analyte that undergoes reduction in two or more steps (e.g., 1,4-benzodiazepine, tetracycline).

The background (residual) current that flows in the absence of the electroactive species of interest is composed of contributions due to double-layer charging process and redox reactions of impurities, as well as of the solvent, electrolyte, or electrode. The latter processes (e.g., hydrogen evolution and mercury oxidation) are those that limit the working potential range. In acidic solutions, the negative background limit shifts by approximately 59 mV per each pH unit to more positive potentials with decreasing pH. Within the working potential window, the charging current is the major component of the background (which limits the detection limit). It is the current required to charge the electrode–solution interface (which acts as a capacitor) on changing the potential or the electrode area (see Section 1.3). Thus, the charging current is present in all conventional polarographic experiments, regardless of the purity of reagents. Because of the negligible potential change during the drop life, the charging associated with the potential scan can be ignored. The value of the polarographic charging current thus depends on the time change of the electrode area:

$$i_c = \frac{dq}{dt} = (E - E_{pzc}) C_{dl} \frac{dA}{dt} \tag{3.12}$$

By substituting the derivative of the area with time [from Eq. (3.2)], one obtains

$$i_c = 0.00567(E - E_{pzc}) C_{dl} m^{2/3} t^{-1/3} \tag{3.13}$$

Hence, the charging current decreases during the drop life, while the diffusion current increases (Fig. 3.4):

$$i_{total}(t) = i_d(t) + i_c(t) = kt^{1/6} + k't^{-1/3} \tag{3.14}$$

The analytical significance of the charging current depends on how large it is relative to the diffusion current of interest. When the analyte concentration is in the 10^{-4}–10^{-2} M range, the current is mostly faradaic, and a well-defined polarographic wave is obtained. However, at low concentrations of the analyte, the charging current contribution becomes comparable to the analytical signal, and the measurement becomes impossible. The charging current thus limits the detection limit of classical polarography to the 5×10^{-6}–1×10^{-5} M region. Lower detection limits are obtained for analytes with redox potentials closer to E_{pzc} [when i_c approaches its smaller value, Eq. (3.12)]. Advanced (pulse) polarographic techniques, discussed in Section 3.3, offer lower detection limits by taking advantage of the different time dependences of the analytical and charging currents [Eq. (3.14)]. Such developments have led to a decrease in the utility of DC polarography.

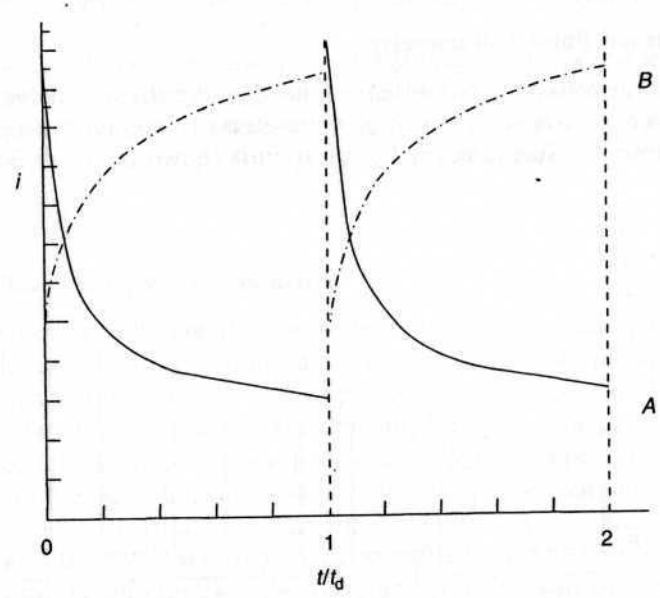

Figure 3.4 Variation of the charging and diffusion currents (*A* and *B*, respectively) during the lifetime of a drop.

3.3 PULSE VOLTAMMETRY

Pulse voltammetric techniques, introduced by Barker and Jenkin (3), are aimed at lowering the detection limits of voltammetric measurements. By substantially increasing the ratio between the faradaic and nonfaradaic currents, such techniques permit convenient quantitation down to the 10^{-8}M concentration level. Because of their greatly improved performance, modern pulse techniques have largely supplanted classical polarography in the analytical laboratory. The various pulse techniques are all based on a sampled current/potential-step (chronoamperometric) experiment. A sequence of such potential steps, each with a duration of about 50ms, is applied onto the working electrode. After the potential is stepped, the charging current decays rapidly (exponentially) to a negligible value, while the faradaic current decays more slowly. Thus, by sampling the current late in the pulse life, an effective discrimination against the charging current is achieved.

The difference between the various pulse voltammetric techniques is the excitation waveform and the current sampling regime. With both normal-pulse and differential-pulse voltammetry, one potential pulse is applied for each drop of mercury when the DME is used. (Both techniques can also be used at solid electrodes.) By controlling the drop time (with a mechanical knocker), the pulse is synchronized with the maximum growth of the mercury drop. At this point, near the end of the drop lifetime, the faradaic current reaches its maximum value, while the contribution of the charging current is minimal (based on the time dependence of the components).

3.3.1 Normal-Pulse Voltammetry

Normal-pulse voltammetry consists of a series of pulses of increasing amplitude applied to successive drops at a preselected time near the end of each drop lifetime (4). Such a normal pulse train is shown in Figure 3.5. Between

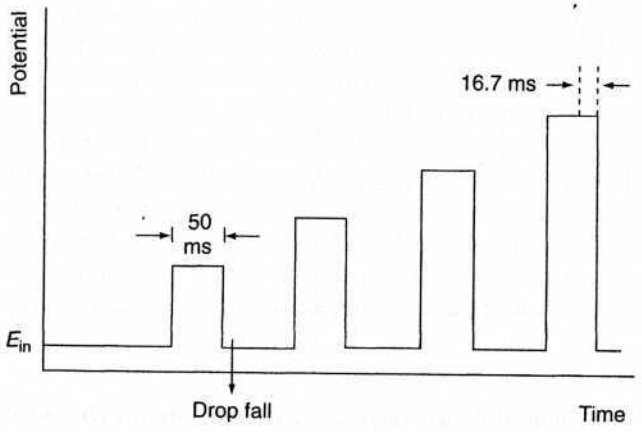

Figure 3.5 Excitation signal for normal-pulse voltammetry.

the pulses, the electrode is kept at a constant (base) potential at which no reaction of the analyte occurs. The amplitude of the pulse increases linearly with each drop. The current is measured about 40ms after the pulse is applied, at which time the contribution of the charging current is nearly zero. In addition, because of the short pulse duration, the diffusion layer is thinner than that of DC polarography (i.e., greater flux of analyte) and hence the faradaic current is increased. The resulting voltammogram has a sigmoidal shape, with a limiting current given by a modified Cottrell equation:

$$i_l = \frac{nFAD^{1/2}C}{\sqrt{\pi t_m}} \tag{3.15}$$

where t_m is the time after application of the pulse where the current is sampled. This current can be compared to that measured in DC polarography:

$$\frac{i_{l,NP}}{i_{l,dc}} = \left(\frac{3t_d}{7t_m}\right)^{1/2} \tag{3.16}$$

This ratio predicts that normal-pulse polarography will be 5–10 times more sensitive than DC polarography (for typical values of t_d and t_m). Normal-pulse polarography may be advantageous also when using solid electrodes. In particular, by maintaining a low initial potential during most of the operation, it is possible to alleviate surface fouling problems (due to adsorbed reaction products).

A related technique, reverse-pulse voltammetry, has a pulse sequence that is a mirror image of that of normal-pulse voltammetry (5). In this case, the initial potential is on the plateau of the wave (i.e., where reduction occurs), and a series of positive-going pulses of decreasing amplitude is applied.

3.3.2 Differential-Pulse Voltammetry

Differential-pulse voltammetry is an extremely useful technique for measuring trace levels of organic and inorganic species. In differential-pulse voltammetry, fixed magnitude pulses—superimposed on a linear potential ramp—are applied to the working electrode at a time just before the end of the drop (Fig. 3.6). The current is sampled twice, just before the pulse application (at 1) and again late in the pulse life (after ~40ms, at 2, when the charging current has decayed). The first current is instrumentally subtracted from the second, and this current difference $[\Delta i = i(t_2) - i(t_1)]$ is plotted against the applied potential. The resulting differential-pulse voltammogram consists of current peaks, the height of which is directly proportional to the concentration of the corresponding analytes:

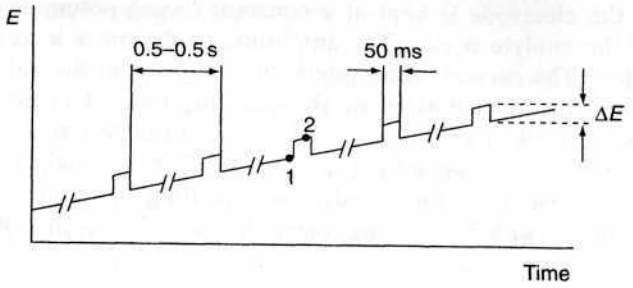

Figure 3.6 Excitation signal for differential-pulse voltammetry.

$$i_p = \frac{nFAD^{1/2}C}{\sqrt{\pi t_m}}\left(\frac{1-\sigma}{1+\sigma}\right) \tag{3.17}$$

where $\sigma = \exp[(nf/RT)(\Delta E/2)]$ (ΔE is the pulse amplitude). The maximum value of the quotient $(1 - \sigma)/(1+ \sigma)$, obtained for large pulse amplitudes, is unity (6).

The peak potential (E_p) can be used to identify the species, as it occurs near the polarographic half-wave potential:

$$E_p = E_{1/2} - \Delta E/2 \tag{3.18}$$

The differential-pulse operation results in a very effective correction of the charging background current. The charging-current contribution to the differential current is negligible, as described by

$$\Delta i_c \simeq -0.00567 C_i\, \Delta E m^{2/3} t^{-1/3} \tag{3.19}$$

where C_i is the integral capacitance. Such background contribution is smaller by more than an order of magnitude than the charging current of normal-pulse voltammetry. Accordingly, differential-pulse voltammetry allows measurements at concentrations as low as 10^{-8}M (about 1 µg/L). The improved detectability over DC polarography is demonstrated in Figure 3.7, which compares the response of both techniques for the antibiotic chloramphenicol present at the 1.3×10^{-5}M level. Similarly, the improvements over normal-pulse polarography are illustrated in Figure 3.8.

The peak-shaped response of differential-pulse measurements results also in improved resolution between two species with similar redox potentials. In various situations, peaks separated by 50 mV may be measured. Such quantitation depends not only on the corresponding peak potentials but also on the widths of the peak. The width of the peak (at half-height) is related to the electron stoichiometry:

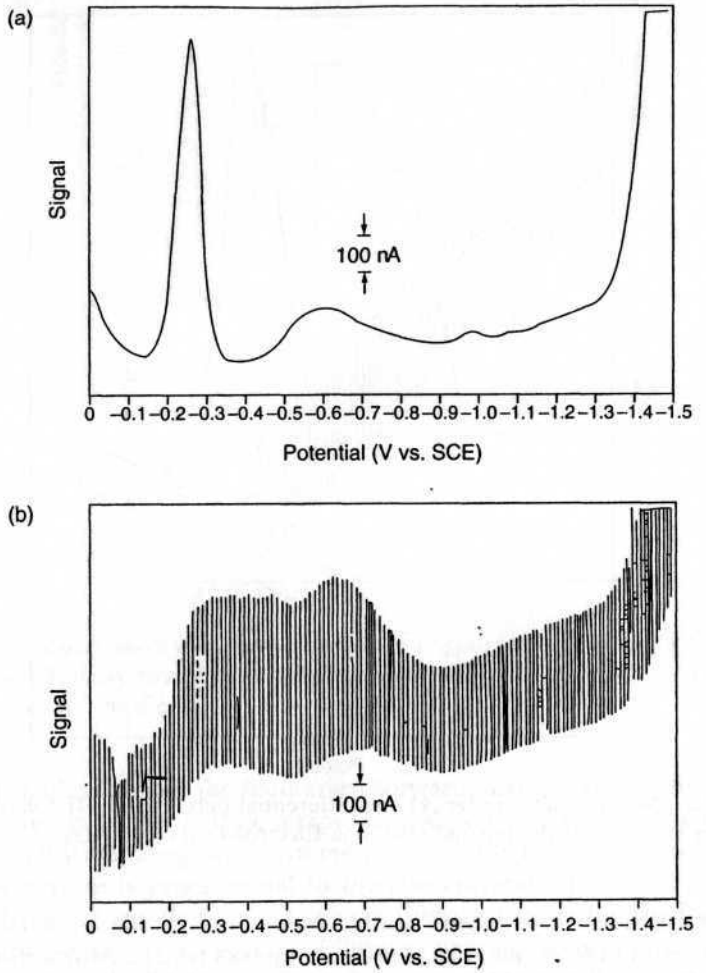

Figure 3.7 Differential-pulse (a) and DC (b) polarograms for a 1.3×10^{-5}M chloramphenicol solution. (Reproduced with permission from Ref. 7.)

$$W_{1/2} = \frac{3.52RT}{nF} \tag{3.20}$$

and thus corresponds to 30.1 mV for $n = 1$ (at 25°C). The peak-shaped response, coupled with the flat background current, makes the technique particularly useful for analysis of mixtures.

The selection of the pulse amplitude and potential scan rate usually requires a tradeoff among sensitivity, resolution, and speed. For example, larger pulse amplitudes result in larger and broader peaks. Pulse amplitudes of 25–50 mV,

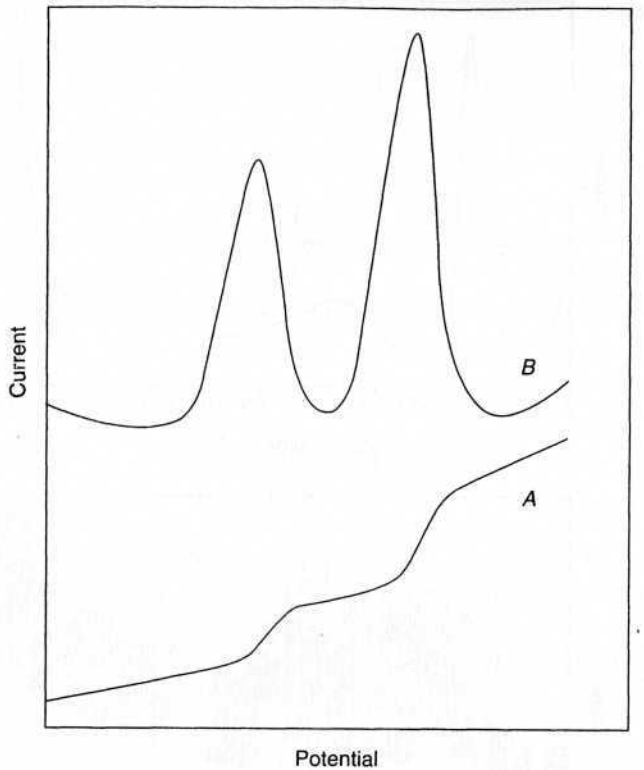

Figure 3.8 Normal-pulse (curve *A*) and differential-pulse (curve *B*) polarograms for a mixture of 1 mg/L cadmium and lead ions. Electrolyte, 0.1 M HNO_3.

coupled with a scan rate of 5 mV/s, are commonly employed. Irreversible redox systems result in lower and broader current peaks (i.e., inferior sensitivity and resolution) compared with those predicted for reversible systems (6). In addition to improvements in sensitivity and resolution, the technique can provide information about the chemical form in which the analyte appears (oxidation states, complexation, etc.).

3.3.3 Square-Wave Voltammetry

Square-wave voltammetry is a large-amplitude differential technique in which a waveform composed of a symmetric square wave, superimposed on a base staircase potential, is applied to the working electrode (8) (Fig. 3.9). The current is sampled twice during each square-wave cycle, once at the end of the forward pulse (at t_1) and once at the end of the reverse pulse (at t_2). Since the square-wave modulation amplitude is very large, the reverse pulses cause the reverse reaction of the product (of the forward pulse). The difference between the two measurements is plotted versus the base staircase potential.

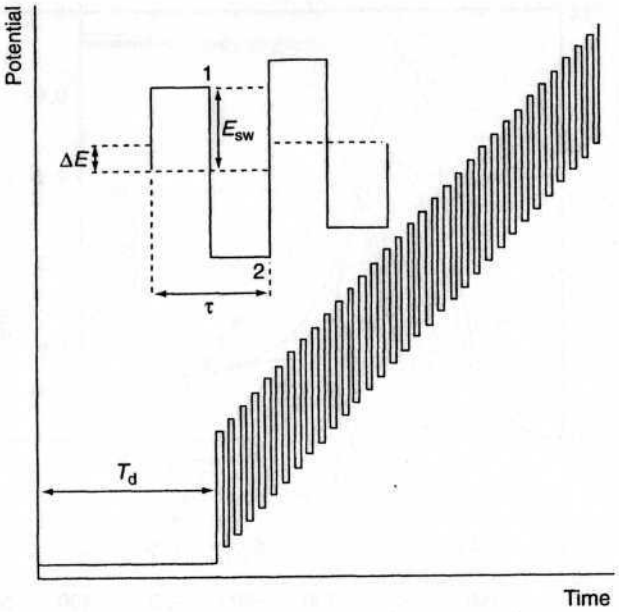

Figure 3.9 Square-wave waveform showing the amplitude E_{sw}, step height ΔE, square-wave period T, delay time T_d, and current measurement times 1 and 2. (Reproduced with permission from Ref. 9.)

A dimensionless plot of the theoretical forward, reverse, and difference currents is given in Figure 3.10 for a rapid reversible redox system. The resulting peak-shaped voltammogram is symmetric about the half-wave potential, and the peak current is proportional to the concentration. Excellent sensitivity accrues from the fact that the net current is larger than either the forward or reverse components (since it is the difference between them); the sensitivity is higher than that of differential pulse polarography (in which the reverse current is not used). Coupled with the effective discrimination against the charging background current, very low detection limits near 1×10^{-8} M can be attained. Comparison between square-wave and differential-pulse voltammetry for reversible and irreversible cases indicated that the square-wave currents are 4 and 3.3 times higher, respectively, than the analogous differential-pulse response (10). Figure 3.11 displays typical square-wave voltammograms obtained at a printed carbon strip electrode for increasing concentrations (1–10 ppm) of the nitroaromatic explosive 2,4,6-trinitrotoluene (TNT) (11).

The major advantage of square-wave voltammetry is its speed. The effective scan rate is given by $f\,\Delta E_s$. The term f is the square-wave frequency (in Hz) and ΔE_s is the step height. Frequencies of 1–100 cycles per second permit the use of extremely fast potential scan rates. For example, if $\Delta E_s = 10$ mV and $f = 50$ Hz, then the effective scan rate is 0.5 V/s. As a result, the analysis time is drastically reduced; a complete voltammogram can be recorded within a few

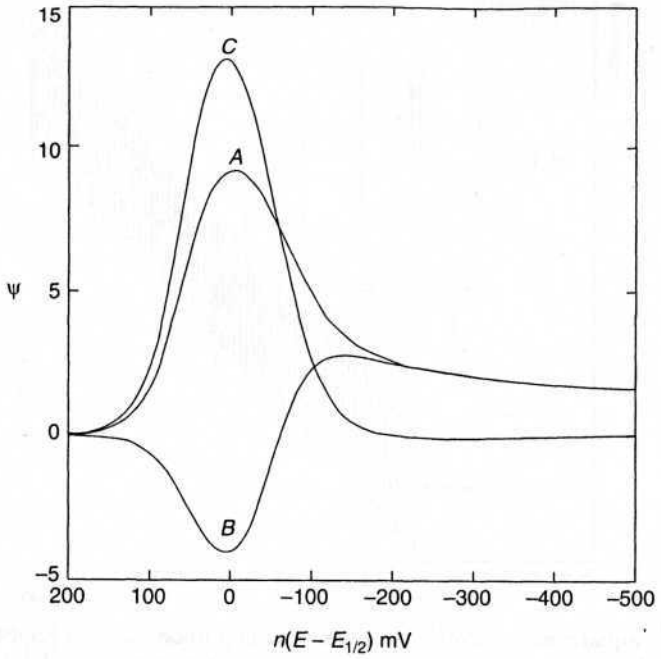

Figure 3.10 Square-wave voltammograms for reversible electron transfer: (curve *A*) forward current; (curve *B*) reverse current; (curve *C*) net current. (Reproduced with permission from Ref. 9.)

seconds, as compared with about 2–3 min in differential-pulse voltammetry. Because of the fast scan rates, the entire voltammogram is recorded on a single mercury drop. Hence, such an operation consumes many drops (compared to other pulse techniques). The inherent speed of square-wave voltammetry can greatly increase sample throughputs in batch (12) and flow (13) analytical operations. In addition, square-wave voltammetric detection for liquid chromatography and capillary electrophoresis can be used to resolve coeluting or comigrating species and assist in peak identification (14, 15). Kinetic studies can also benefit from the rapid scanning capability and the reversal nature of square-wave voltammetry.

3.3.4 Staircase Voltammetry

Staircase voltammetry has been proposed as a useful tool for rejecting the background charging current. The potential–time waveform involves successive potential steps of ~10 mV height and about 50 ms duration (Fig. 3.12). The current is sampled at the end of each step, where the charging current has decayed to a negligible value. Hence, this waveform couples the discrimination against the charging current with the experimental speed of linear scan voltammetry. Such an operation results in a peak-shaped current response, similar to that of linear scan experiments. Indeed, as the steps become smaller,

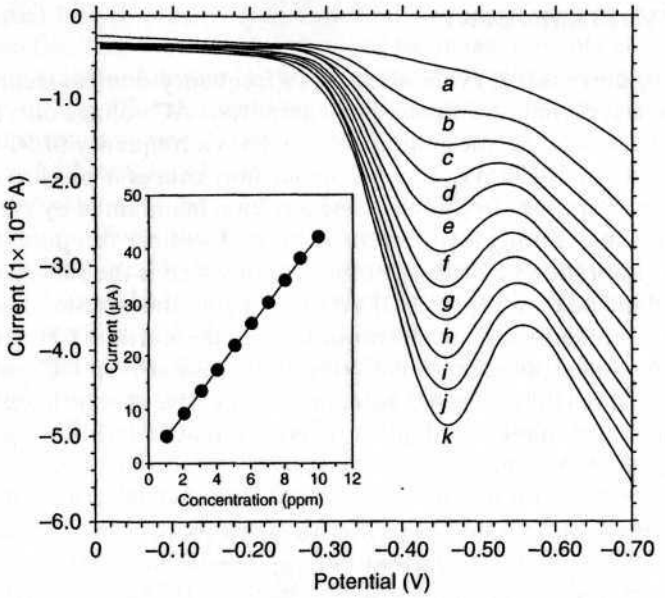

Figure 3.11 Square-wave voltammograms for TNT solutions of increasing concentration from 1 to 10 ppm (curves *b*–*k*), along with the background voltammogram (curve *a*) and resulting calibration plot (inset). (Reproduced with permission from Ref. 11.)

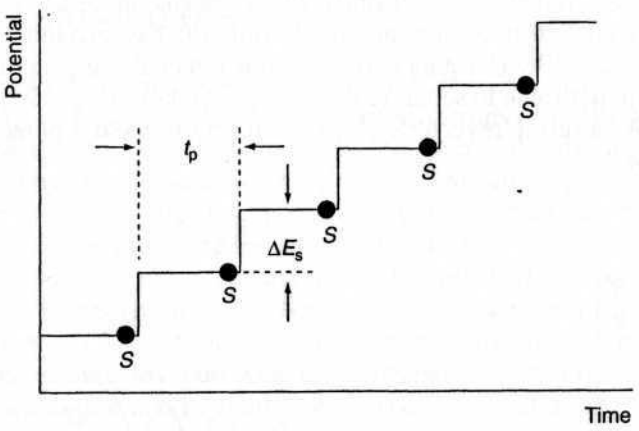

Figure 3.12 Potential–time waveform used in staircase voltammetry.

the equations for the staircase voltammetric response converge with those of linear scan voltammetry (16). As such, staircase voltammetry can be considered as the digital version of linear scan voltammetry. Similarly, cyclic staircase voltammetric experiments, in which the direction of the potential steps is reversed at a switching potential, result in a voltammetric response resembling cyclic voltammetry (but with a much reduced charging-current contribution).

3.4 AC VOLTAMMETRY

Alternating current (AC) voltammetry is a frequency-domain technique which involves the superimposition of a small amplitude AC voltage on a linear ramp (Fig. 3.13). Usually the alternating potential has a frequency of 50–100 Hz and an amplitude of 10–20 mV. The AC signal thus causes a perturbation in the surface concentration, around the concentration maintained by the DC potential ramp. The resulting AC current is plotted against the potential. Such a voltammogram shows a peak, the potential of which is the same as that of the polarographic half-wave potential. (At this region the sinusoid has maximum impact on the surface concentration, i.e., on the current.) For a reversible system, such a response is actually the derivative of the DC polarographic response. The height of the AC voltammetric peak is proportional to the concentration of the analyte and, for a reversible reaction, to the square root of the frequency (ω):

$$i_p = \frac{n^2F^2A\omega^{1/2}D^{1/2}C\Delta E}{4RT} \tag{3.21}$$

The term ΔE is the amplitude. The peak width is independent of the AC frequency, and is $90.4/n$ mV (at 25°C).

The detection of the ac component allows one to separate the contributions of the faradaic and charging currents. The former is phase-shifted by 45° relative to the applied sinusoidal potential, while the background component is 90° out of phase. The charging current is thus rejected using a phase-sensitive lock-in amplifier (able to separate the in-phase and out-of-phase current components). As a result, reversible electrode reactions yield a detection limit of ~5×10^{-7} M.

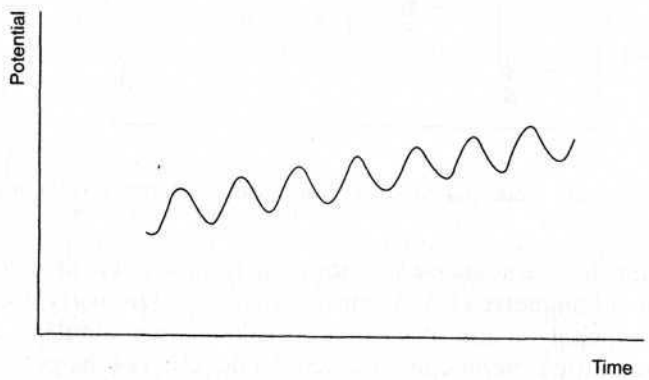

Figure 3.13 Potential-time waveform used in alternating current (ac) voltammetry.

Substantial loss in sensitivity is expected for analytes with slow electron transfer kinetics. This may be advantageous for measurements of species with fast electron transfer kinetics in the presence of one (e.g., dissolved oxygen) that is irreversible. (For the same reason, the technique is very useful for the study of electron processes.) Theoretical discussions on AC voltammetry are available in the literature (17–19).

Large-amplitude sine waves have been combined with conversion of the raw time domain (from the electrochemical cell) into the frequency domain (20,21). Such frequency-based sinusoidal voltammetry offers decoupling of the faradaic signal from the background components (i.e., lower detection limits), as well as generation of a distinct "fingerprint" frequency spectrum to aid in the identification of specific chemical molecules (20). Such decoupling of the faradaic signal reflects the fact that at large (i.e., >50 mV) amplitudes of the applied potential, it exhibits an intensity at higher order harmonics of the fundamental excitation frequency, as compared to the capacitive charging current that remains at the fundamental frequency. In addition to improved sensitivity at higher harmonics, redox species with different electrochemical properties can be detected selectively on the basis of their unique "fingerprint" frequency response (20,22). For example, measurements in the presence of dissolved oxygen have been accomplished on the basis of kinetic discrimination against the oxygen reduction process (22).

3.5 STRIPPING ANALYSIS

Stripping analysis is an extremely sensitive electrochemical technique for measuring trace metals (23,24). Its remarkable sensitivity is attributed to the combination of an effective preconcentration step with advanced measurement procedures that generates an extremely favorable signal : background ratio. Since the metals are preconcentrated into the electrode by factors of 100–1000, detection limits are lowered by two to three orders of magnitude compared to solution-phase voltammetric measurements. Hence, four to six metals can be measured simultaneously in various matrices at concentration levels down to 10^{-10} M, utilizing relatively inexpensive instrumentation. The ability to obtain such low detection limits strongly depends on the degree to which contamination can be minimized. Expertise in ultratrace chemistry is required.

Essentially, stripping analysis is a two-step technique. The first, or deposition step, involves the electrolytic deposition of a small portion of the metal ions in solution into the mercury electrode to preconcentrate the metals. This is followed by the stripping step (the measurement step), which involves the dissolution (stripping) of the deposit. Different versions of stripping analysis can be employed, depending on the nature of the deposition and measurement steps.

3.5.1 Anodic Stripping Voltammetry

Anodic stripping voltammetry (ASV) is the most widely used form of stripping analysis. In this case, the metals are being preconcentrated by electrodeposition into a small-volume mercury electrode (a thin mercury film or a hanging mercury drop). The preconcentration is done by cathodic deposition at a controlled time and potential. The deposition potential is usually 0.3–0.5 V more negative than E° for the least easily reduced metal ion to be determined. The metal ions reach the mercury electrode by diffusion and convection, where they are reduced and concentrated as amalgams:

$$M^{n+} + ne^- + Hg \rightarrow M(Hg) \tag{3.22}$$

The convective transport is achieved by electrode rotation or solution stirring (in conjunction with the mercury film electrode) or by solution stirring (when using the hanging mercury drop electrode). Quiescent solutions can be used when using mercury ultramicroelectrodes. The duration of the deposition step is selected according to the concentration level of the metal ions in question, from less than 0.5 min at the 10^{-7} M level to about 20 min at the 10^{-10} M level. The concentration of the metal in the amalgam, C_{Hg}, is given by Faraday's law

$$C_{Hg} = \frac{i_l t_d}{nFV_{Hg}} \tag{3.23}$$

where i_l is the limiting current for the deposition of the metal, t_d is the length of the deposition period, and V_{Hg} is the volume of the mercury electrode. The deposition current is related to the flux of the metal ion at the surface. The total amount of metal plated represents a small (and yet reproducible) fraction of the metal present in the bulk solution.

Following the preselected time of the deposition, the forced convection is stopped, and the potential is scanned anodically, linearly, or in a more sensitive potential–time (pulse) waveform that discriminates against the charging background current (usually square-wave or differential-pulse ramps). Such pulse excitations also offer reduced oxygen interferences and analyte replating, respectively. During this anodic scan, the amalgamated metals are reoxidized, stripped out of the electrode (in an order that is a function of each metal standard potential), and an oxidation (stripping) current is flowing:

$$M(Hg) \rightarrow M^{n+} + ne^- + Hg \tag{3.24}$$

Repetitive ASV runs can be performed with good reproducibility in connection to a short (30–60-s) "electrochemical cleaning" period at the final potential (e.g., +0.1 V using mercury electrodes). The potential–time sequence used in ASV, along with the resulting stripping voltammogram, is shown in Figure

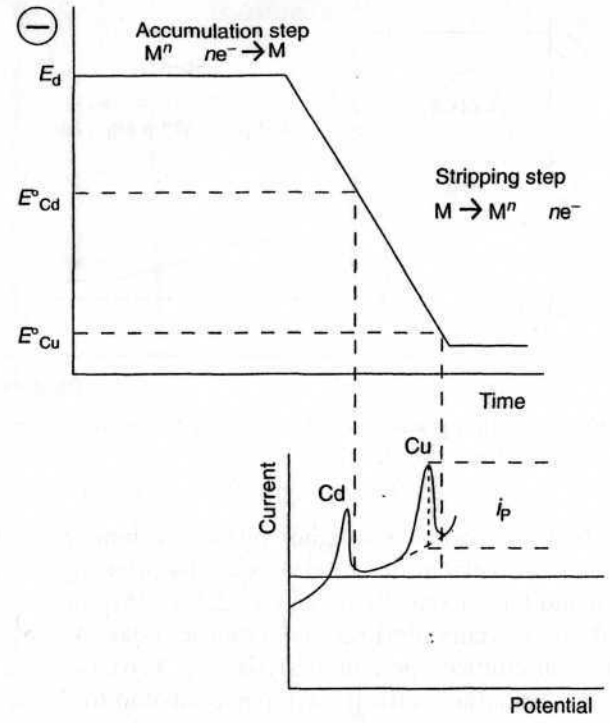

Figure 3.14 Anodic stripping voltammetry: the potential–time waveform (top), along with the resulting voltammogram (bottom).

3.14. The voltammetric peak reflects the time-dependent concentration gradient of the metal in the mercury electrode during the potential scan. Peak potentials serve to identify the metals in the sample. The peak current depends on various parameters of the deposition and stripping steps, as well as on the characteristics of the metal ion and the electrode geometry. For example, for a mercury film electrode, the peak current is given by

$$i_p = \frac{n^2F^2v^{1/2}AlC_{Hg}}{2.7RT} \tag{3.25}$$

where A and l are the area and thickness, respectively, of the film and v is the potential scan rate (during the stripping). The corresponding concentration profile in the film and nearby solution is displayed in Figure 3.15. (For very thin mercury films, diffusion in the film can be ignored and the peak current will be directly proportional to the scan rate.) For the hanging mercury drop, the following expression describes the stripping peak current:

$$i_p = 2.72 \times 10^5 n^{3/2} A D^{1/2} v^{1/2} C_{Hg} \tag{3.26}$$

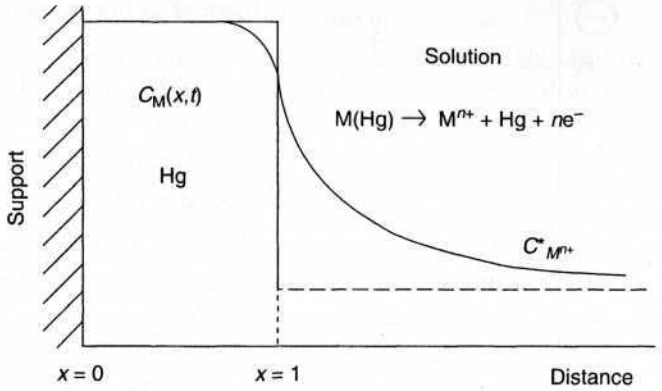

Figure 3.15 Concentration gradient of the metal in the mercury film electrode and nearby solution during the stripping step.

The mercury film electrode has a higher surface : volume ratio than does the hanging mercury drop electrode and consequently offers a more efficient preconcentration and higher sensitivity [Eqs. (3.23)–(3.26)]. In addition, the total exhaustion of thin mercury films results in sharper peaks and hence improved peak resolution in multicomponent analysis (Fig. 3.16). Because of the toxicity of mercury, considerable efforts have been devoted to the investigation of alternate electrode materials. Among the proposed alternative ("mercury-free") electrodes, the bismuth one offers the closest behavior to mercury (27,28). Both in-situ or preplated bismuth-film and bulk bismuth electrodes display a very attractive stripping behavior. Such behavior reflects the ability of bismuth to form "fused" multicomponent alloys with heavy metals. Gold electrodes have been particularly useful for stripping measurements of important trace metals (e.g., Hg, As, Se) with oxidation potentials more positive than those of mercury or bismuth. The combination of ultrasound with stripping voltammetry, has been proposed to allow the possibility of a wider use of solid electrodes and to overcome electrode passivation in real samples (29).

The major types of interferences in ASV procedures are overlapping stripping peaks caused by a similarity in the oxidation potentials (e.g., of the Pb, Tl, Cd, Sn or Bi, Cu, Sb groups), the presence of surface-active organic compounds that adsorb on the mercury electrode and inhibit the metal deposition, and the formation of intermetallic compounds (e.g., Cu–Zn), which affects the peak size and position. Knowledge of these interferences can lead to their prevention, through adequate attention to key operations.

Improved signal-to-background characteristics can be achieved using dual-working electrode techniques, such as ASV with collection or subtractive ASV (but at the expense of more complex instrumentation).

Other versions of stripping analysis, including potentiometric stripping, adsorptive stripping, and cathodic stripping schemes, have been developed to further expand its scope and power.

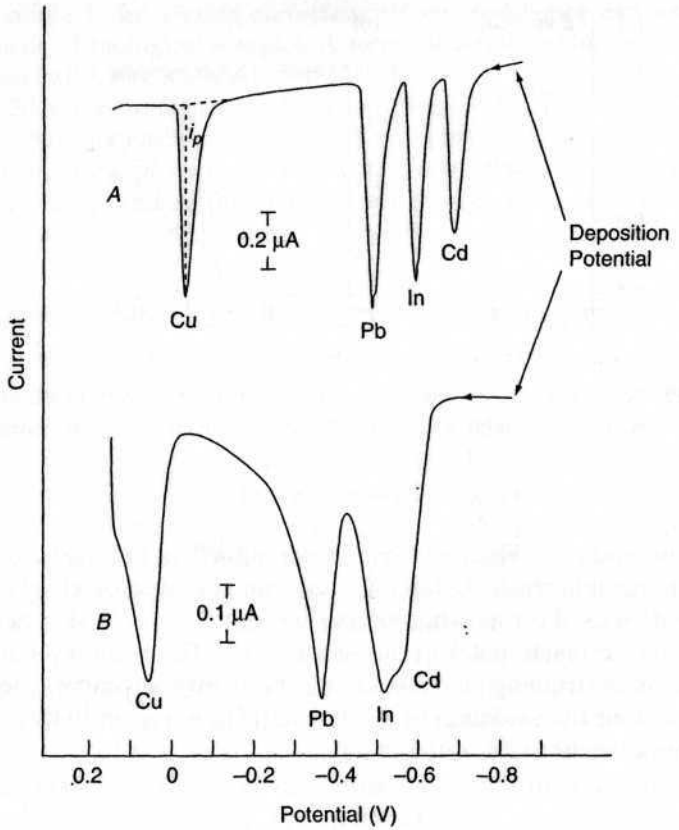

Figure 3.16 Stripping voltammograms for 2×10^{-7}M Cu^{2+}, Pb^{2+}, In^{3+}, and Cd^{2+} at the mercury film (*A*) and hanging mercury drop (*B*) electrodes. (Reproduced with permission from Ref. 25.)

3.5.2 Potentiometric Stripping Analysis

Potentiometric stripping analysis (PSA), known also as *stripping potentiometry*, differs from ASV in the method used for stripping the amalgamated metals (30). In this case, the potentiostatic control is disconnected following the preconcentration, and the concentrated metals are reoxidized by an oxidizing agent [e.g., O_2, Hg(II)] that is present in the solution:

$$M(\text{Hg}) + \text{oxidant} \rightarrow M^{n+} \tag{3.27}$$

A stirred solution is used also during the stripping step to facilitate the transport of the oxidant. Alternately, the oxidation can be carried out by passing a constant anodic current through the electrode. During the oxidation step, the variation of the working electrode potential is recorded, and a stripping curve,

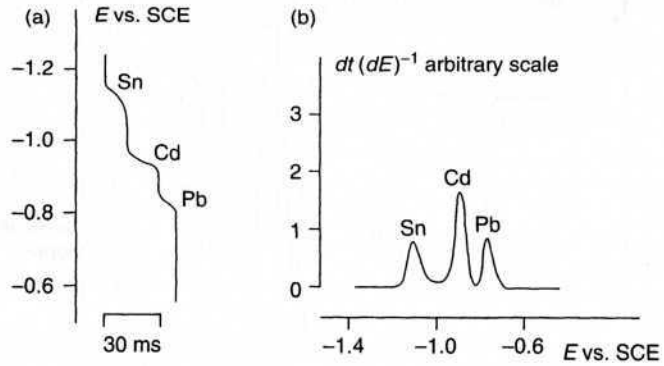

Figure 3.17 Stripping potentiograms for a solution containing 100 µg/L tin, cadmium, and lead, with 80-s accumulation at −1.40 V. (Reproduced with permission from Ref. 30.)

like the one shown in Figure 3.17a, is obtained. When the oxidation potential of a given metal is reached, the potential scan is slowed down as the oxidant (or current) is used for its stripping. A sharp potential step thus accompanies the depletion of each metal from the electrode. The resulting potentiogram thus consists of stripping plateaus, as in a redox titration curve. The transition time needed for the oxidation of a given metal t_M is a quantitative measure of the sample concentration of the metal

$$t_M \propto C_{M^{n+}} t_d / C_{ox} \tag{3.28}$$

where C_{ox} is the concentration of the oxidant. Hence, the signal may be increased by decreasing the oxidant concentration. The qualitative identification relies on potential measurements (in accordance with the Nernst equation for the amalgamated metal):

$$E = E^\circ + \frac{RT}{nF} \ln[M^{n+}]/M(Hg) \tag{3.29}$$

where E° denotes the standard potential for the redox couple $M^{n+}/M(Hg)$.

Modern PSA instruments use microcomputers to register fast stripping events and to convert the wave-shaped response to a more convenient peak over a flat baseline. Such differential display of dt/dE versus E is shown in Figure 3.17b. The use of nondeaerated samples represents an important advantage of PSA (over analogous ASV schemes), particularly in field applications. In addition, such potential–time measurements eliminate the need for amplification when microelectrodes are concerned. By obviating the need for stirring or deoxygenating the solution, the coupling of PSA with microelectrodes permits convenient trace analysis of very small (5-µL) samples. PSA is also

less susceptible to interfering surfactant effects, and hence can simplify the pretreatment of biological samples. A more detailed treatment of the theoretical foundation of PSA is given in Ref. 30.

About 20 amalgam-forming metals, including Pb, Sn, Cu, Zn, Cd, Bi, Sb, Tl, Ga, In, and Mn, are easily measurable by stripping strategies (ASV and PSA) based on cathodic deposition onto mercury electrodes. Additional metals, such as Se, Hg, Ag, Te, and As, are measurable at bare solid electrodes such as carbon or gold.

3.5.3 Adsorptive Stripping Voltammetry and Potentiometry

Adsorptive stripping analysis greatly enhances the scope of stripping measurements toward numerous trace elements (31–33). This relatively new strategy involves the formation, adsorptive accumulation, and reduction of a surface-active complex of the metal (Fig. 3.18). Both voltammetric and potentiometric stripping schemes, with a negative-going potential scan or constant cathodic current, respectively, can be employed for measuring the adsorbed complex. Most procedures involve the reduction of the metal in the adsorbed complex (although it is also possible to exploit the reduction of the ligand). The response of the surface-confined species is directly related to its surface concentration, with the adsorption isotherm (commonly that of Langmuir—discussed in Section 2.1), providing the relationship between the surface and bulk concentrations of the adsorbate. As a result, calibration curves display nonlinearity at high concentrations. The maximum adsorption density is related to the size and surface concentration of the adsorbed complex.

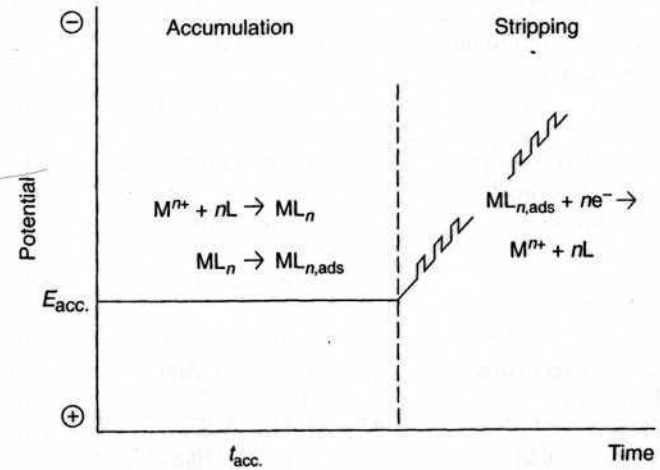

Figure 3.18 Accumulation and stripping steps in adsorptive stripping measurements of a metal ion (M^{n+}) in the presence of an appropriate chelate agent (L).

Short adsorption times (1–5 min) result in a very effective interfacial accumulation. The reduction step is also very efficient as the entire collected complex is reduced. Such a combination thus results in extremely low detection limits (10^{-10}–10^{-11} M) for important metals, including uranium, vanadium, aluminum, or molybdenum. Even lower levels, for example, 10^{-12} M of platinum, titanium, cobalt, chromium, or iron, can be measured by coupling the adsorption accumulation with catalytic reactions. In this case, the response of the accumulated complex is greatly amplified through a catalytic cycle, for example, in the presence of an oxidant. The adsorptive approach may also offer improvements in selectivity or sensitivity for metals (e.g., tin, nickel) that are measurable also by conventional stripping analysis. Examples of adsorptive stripping schemes for measuring trace metals are listed in Table 3.2. All procedures rely on a judicious choice of chelating agent. The resulting complex should be surface active and electroactive; in addition, selective complexation can be used to enhance the overall selectivity.

Besides trace metals, adsorptive stripping voltammetry has been shown to be highly suitable for measuring organic compounds (including cardiac or anticancer drugs, nucleic acids, vitamins, or pesticides) that exhibit surface-active properties. Depending on their redox activity, the quantitation of the adsorbed organic compounds may proceed, through oxidation or reduction. For example, modern adsorptive stripping voltammetric and potentiometric methods represent highly sensitive tools for detecting ultratrace levels of nucleic acids. Figure 3.19 displays the adsorptive stripping potentiometric

TABLE 3.2 Common Adsorptive Stripping Schemes for Measurements of Trace Metals

Metal	Complexing Agent	Supporting Electrolyte	Detection Limit (M)	Ref.
Al	Di(hydroxyanthraquinone sulfonic acid)	BES buffer	1×10^{-9}	34
Be	Thorin	Ammonia buffer	3×10^{-9}	35
Co	Nioxime	HEPES buffer	6×10^{-12}	36
Cr	Diethylenetriamine-pentaacetic acid	Acetate buffer	4×10^{-10}	37
Fe	Solochrome violet RS	Acetate buffer	7×10^{-10}	38
Mn	Eriochrome Black T	PIPES buffer	6×10^{-10}	39
Mo	Oxine	Hydrochloric acid	1×10^{-10}	40
Ni	Dimethylglyoxime	Ammonia buffer	1×10^{-10}	41
Pt	Formazone	Sulfuric acid	1×10^{-12}	42
Sn	Tropolone	Acetate buffer	2×10^{-10}	43
Ti	Mandelic acid	Potassium chlorate	7×10^{-12}	44
U	Oxine	PIPES buffer	2×10^{-10}	45
V	Catechol	PIPES buffer	1×10^{-10}	46

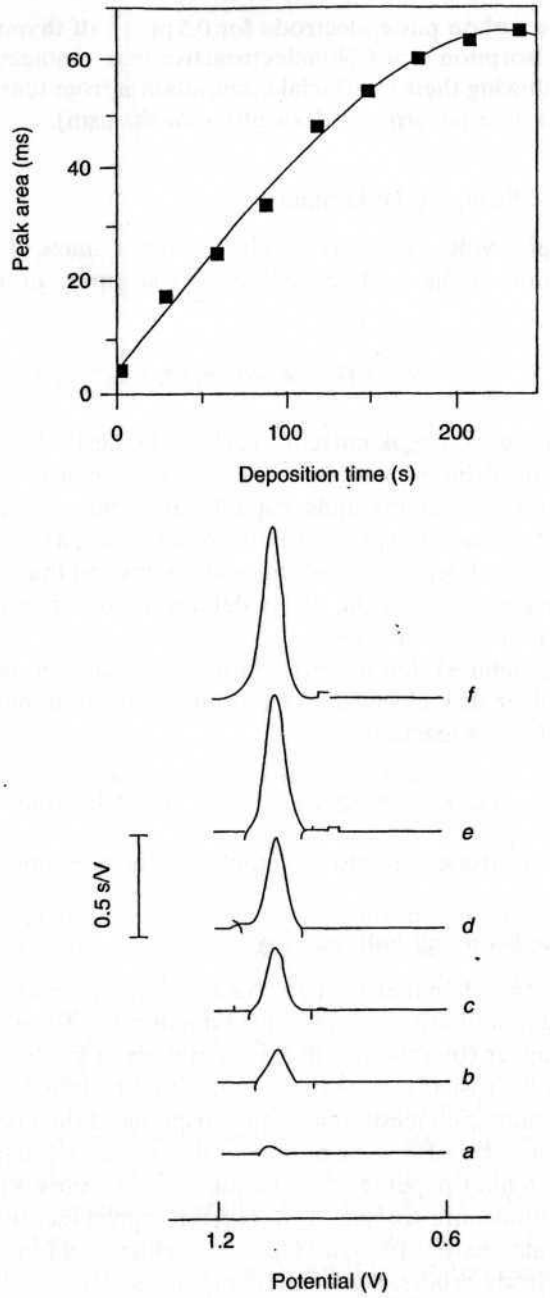

Figure 3.19 Adsorptive stripping potentiograms for 0.5 ppm calf thymus DNA following different adsorption times: 1–150 s (*a–f*). (Reproduced with permission from Ref. 47.)

response of the carbon paste electrode for 0.5 ppm calf thymus DNA following different adsorption times. Nonelectroactive macromolecules may also be determined following their interfacial accumulation from tensammetric peaks (resulting from their adsorption–desorption mechanism).

3.5.4 Cathodic Stripping Voltammetry

Cathodic stripping voltammetry (CSV) is the mirror image of ASV. It involves anodic deposition of the analyte, followed by stripping in a negative-going potential scan:

$$A^{n-} + Hg \underset{\text{stripping}}{\overset{\text{deposition}}{\rightleftharpoons}} HgA + ne^- \qquad (3.30)$$

The resulting reduction peak current provides the desired quantitative information. Cathodic stripping voltammetry is used to measure a wide range of organic and inorganic compounds, capable of forming insoluble salts with mercury. Among these are various thiols or penicillins, as well as halide ions, cyanide, and sulfide. Highly sensitive measurements can thus be performed, as illustrated in Figure 3.20 for the direct determination of subnanomolar concentrations of iodide in seawater.

Anions (e.g., halides) that form insoluble silver salts can be measured also at a rotating silver disk electrode. In this, the deposition and stripping steps involve the following reaction:

$$Ag + X^- \rightleftharpoons AgX + e^- \qquad X^- = Cl^-, Br^- \qquad (3.31)$$

Copper-based electrodes can also be employed for the same task.

3.5.5 Abrasive Stripping Voltammetry

Abrasive striping voltammetry, introduced by Scholz' team (49), provides a qualitative and quantitative analysis of solid materials. The method involves a mechanical transfer (by rubbing) of trace amounts of a solid sample onto the electrode surface (usually a paraffin-impregnated graphite electrode), followed by voltammetric measurement and stripping of the accumulated material. After the voltammetric measurement, the surface is "cleaned" by rubbing it onto a smooth filter paper. The technique has been shown useful for different aspects of solid-state analysis, including fingerprint identification of alloys, study of minerals, analysis of pigments or pesticides, and fundamental investigations of electrode processes of solid compounds.

3.5.6 Applications

The remarkable sensitivity, broad scope, and low cost of stripping analysis have led to its application in a large number of analytical problems. As illustrated

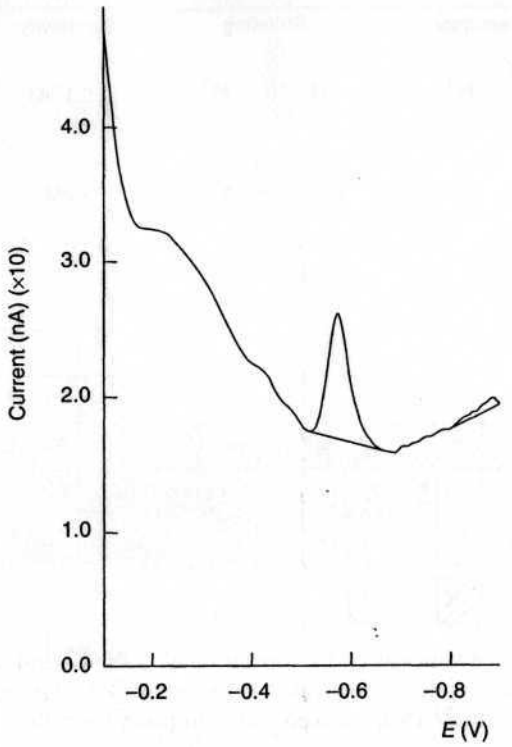

Figure 3.20 Stripping voltammograms for trace iodide in seawater. (Reproduced with permission from Ref. 48.)

in Figure 3.21, over 30 trace elements can be conveniently measured in various matrices by the various versions of stripping analysis. The technique has thus proved useful for the determination of numerous trace metals in environmental, industrial, and clinical samples, as well as for assays of foodstuffs, beverages, gunshot residues, and pharmaceutical formulations. Selected applications are listed in Table 3.3. Figure 3.22 displays adsorptive stripping voltammograms for chromium in various environmental (soil and groundwater) samples from contaminated nuclear energy sites. Stripping analysis has also been an important technique for screening for blood lead in children (58) and for monitoring arsenic in various water samples (67). Many other unique applications of stripping analysis, including studies of metal speciation (oxidation state, metal–ligand interactions) in natural waters, on-line monitoring of industrial processes, in situ oceanographic surveys, or remote environmental sensing, have been reported and reviewed (50,68–70). The technique has also been extremely useful for monitoring metal tags (including nanoparticle tracers) in connection with bioaffinity assays of DNA and proteins (see Ref. 71 and Chapter 6, below).

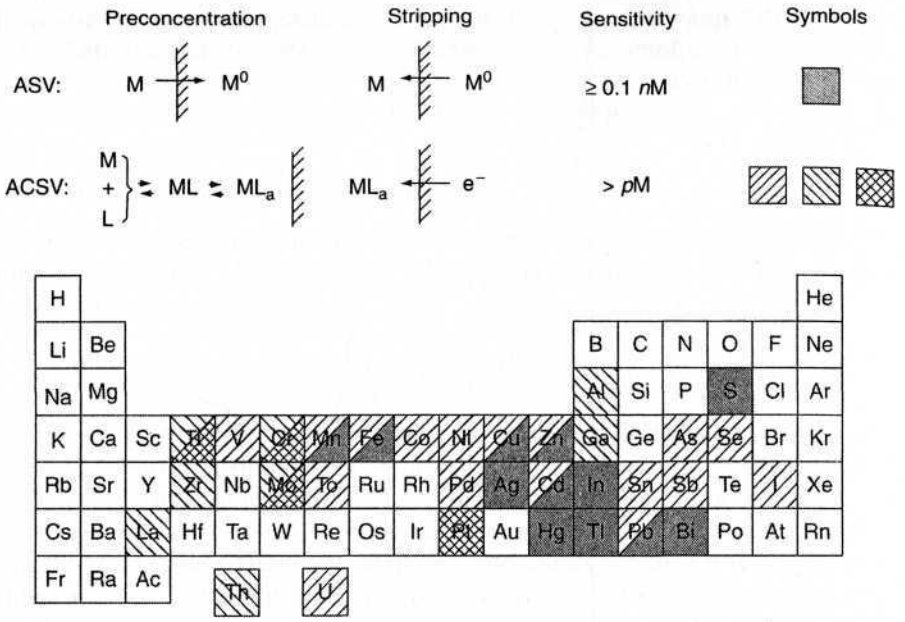

Figure 3.21 Elements measured by conventional ASV and adsorptive stripping schemes with reduction of the element in the complex, reduction of the ligand, or a catalytic process. (Reproduced with permision from Ref. 50.)

TABLE 3.3 Representative Applications of Stripping Analysis

Metal	Sample Matrix	Stripping Mode	Working Electrode	Ref.
Antimony	Gunshot residue	ASV	MFE	51
Cadmium	Lake water	ASV	MFE	52
Chromium	Soil	AdSV	HMDE	53
Cobalt	Soil	AdSV	Bismuth	54
Copper	Steel	ASV	HMDE	55
Iodide	Seawater	CSV	HMDE	48
Iron	Wine	AdSV	HMDE	56
Iron	Seawater	Catalytic AdSV	HMDE	57
Lead	Blood	PSA	MFE	58
Lead	Paint	ASV	—	59
Mercury	Fish	ASV	Au	60
Nickel	Plant leaves	AdSV	HMDE	61
Platinum	Gasoline	AdSV	HMDE	62
Selenium	Soil	CSV	HMDE	63
Thallium	Urine	ASV	HMDE	64
Titanium	Seawater	AdSV	HMDE	44
Uranium	Groundwater	AdSV	HMDE	65
Zinc	Eye tissue	ASV	HMDE	66

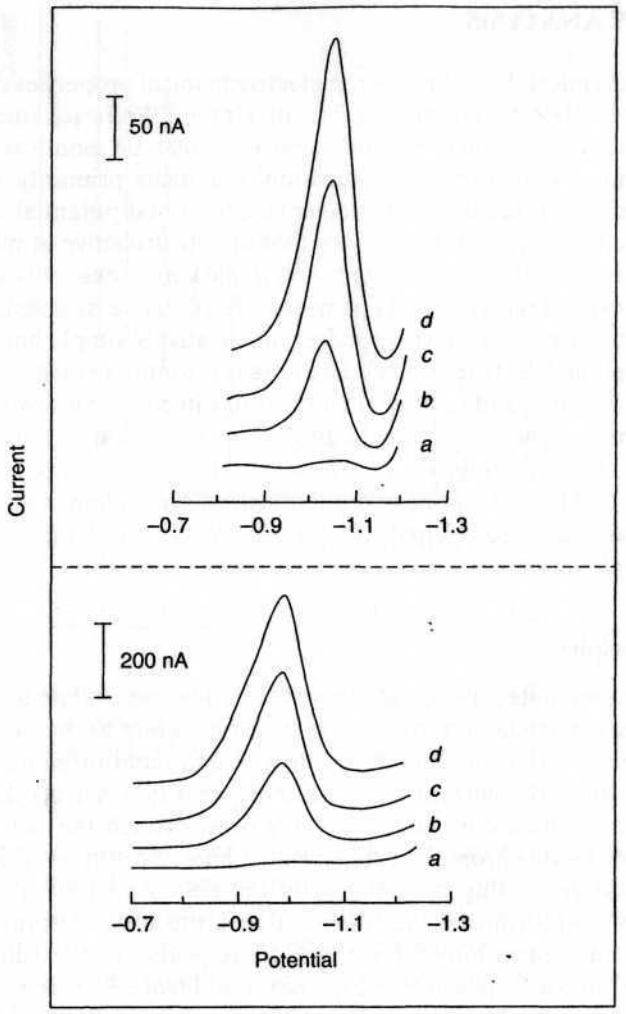

Figure 3.22 Adsorptive stripping voltammograms of chromium in groundwater (top) and soil (bottom) samples, using cupferron as a chelating agent. Top: curve *a*, response for electrolyte; curve *b*, same as curve *a* but after spiking 20 µL of the sample (500-fold dilution); curves *c* and *d*, same as curve *b*, but after additions of 0.1 µg/L chromium; 20 s adsorption. Bottom: curve *a*, response for the electrolyte; curve *b*, same as curve *a* but after spiking 5 µL of the soil extract (2000-fold dilution); curves *c* and *d*, same as curve *b* but after additions of 0.5 µ/L chromium; 15 s adsorption. (Reproduced with permission from Ref. 53.)

3.6 FLOW ANALYSIS

An electrochemical detector uses the electrochemical properties of target analytes for their determination in a flowing stream. While parameters such as current, potential, conductivity, and capacitance can be monitored by various electrochemical detectors, our discussion will focus primarily on the most popular constant-potential measurements. Controlled-potential detectors are ideally suited for monitoring analytes that are electroactive at modest potentials. Such devices are characterized by a remarkable sensitivity (down to the picogram level), high selectivity (toward electroactive species), wide linear range, low dead volumes, fast response, and relatively simple and inexpensive instrumentation. Electrochemical detectors are commonly used in many clinical, environmental, and industrial laboratories in connection with automated flow systems (e.g., flow injection analyzers) or separation techniques [particularly liquid chromatography, conventional and microchip capillary zone electrophoresis (CZE) and on-line microdialysis]. Such coupling of electrochemical detectors with advanced separation steps allows electroanalysis to address highly complex samples.

3.6.1 Principles

Electrochemical detection is usually performed by controlling the potential of the working electrode at a fixed value (corresponding to the limiting current plateau region of the compounds of interest) and monitoring the current as a function of time. The current response thus generated reflects the concentration profiles of these compounds as they pass through the detector. Hence, detection for liquid chromatography or flow injection systems results in sharp current peaks (reflecting the passage of the eluted analyte or sample zone, respectively). Accordingly, the magnitude of the peak current serves as a measure of the concentration. Typical response peaks recorded during an automated flow injection operation are displayed in Figure 3.23. The current peaks are superimposed on a constant background current (caused by redox reactions of the mobile phase or carrier solutions). Larger background currents, expected at high potentials, result in increased (flow rate-dependent) noise level. In particular, the cathodic detection of reducible species is hampered by the presence of traces of oxygen in the flowing solution. Such background noise is strongly influenced by the pulsation of the pump.

The applied potential affects not only the sensitivity and signal : noise characteristics, but also the selectivity of amperometric measurements. In general, a lower potential is more selective and a higher one, more universal. Thus, compounds undergoing redox potentials at lower potentials can be detected with greater selectivity. For example, Figure 3.24 displays electropherograms for a beer sample recorded at different detection potentials. Far fewer peaks are seen in the lower-potential (850 mV) electropherogram. However, the detection potential must be sufficient high to oxidize (or reduce) the compounds of interest. Selection of the applied potential relies on the construction of hydrodynamic voltammograms. These can be obtained by making repeated flow injections of the analyte solution while recording the current at different potentials. The resulting voltammogram has a characteristic wave (sigmoidal) shape. Although it is common to operate the detector on the limiting-current plateau region, a lowering of the operating potential (to the rising portion of the wave) can be used to improve the selectivity and lower the detection limit. Comparison of hydrodynamic voltammograms for the sample and standard solutions can provide important qualitative information.

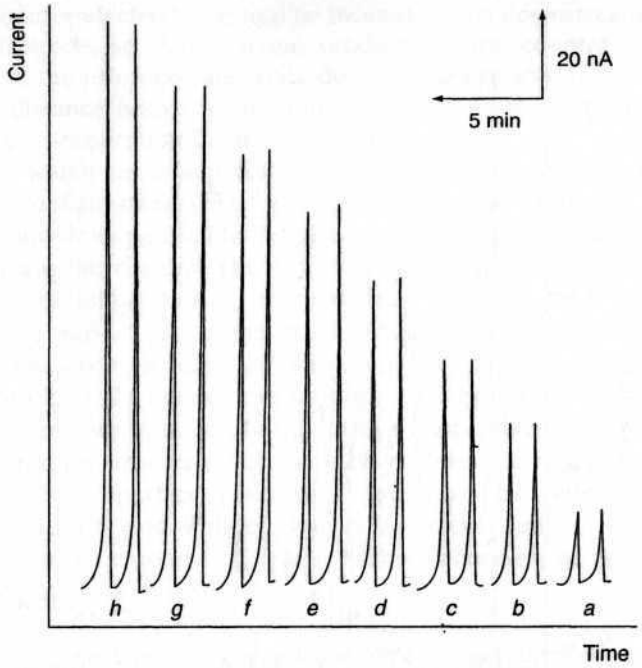

Figure 3.23 Typical amperometric (readout during automated flow injection assays of ethanol solutions of increasing concentrations in 2×10^{-5} M steps at a carbon paste enzyme electrode detector. Curves *a–h*: 2×10^{-5} M – 1.6×10^{-4} M ethanol.

Depending on their conversion efficiency, electrochemical detectors can be divided into two categories: those that electrolyze only a negligible fraction (0.1–5%) of the electroactive species passing through the detector (amperometric detectors), and those for which the conversion efficiency is approaching 100% (coulometric detectors). Unfortunately, the increased conversion efficiency of the analyte is accompanied by a similar increase for the electrolyte (background) reactions, and no lowering of detection limits is realized.

Various (pre- or postcolumn) chemical and biochemical derivatization schemes have thus been employed for expanding the scope of electrochemical detectors toward electroinactive analytes (through the introduction of elec-

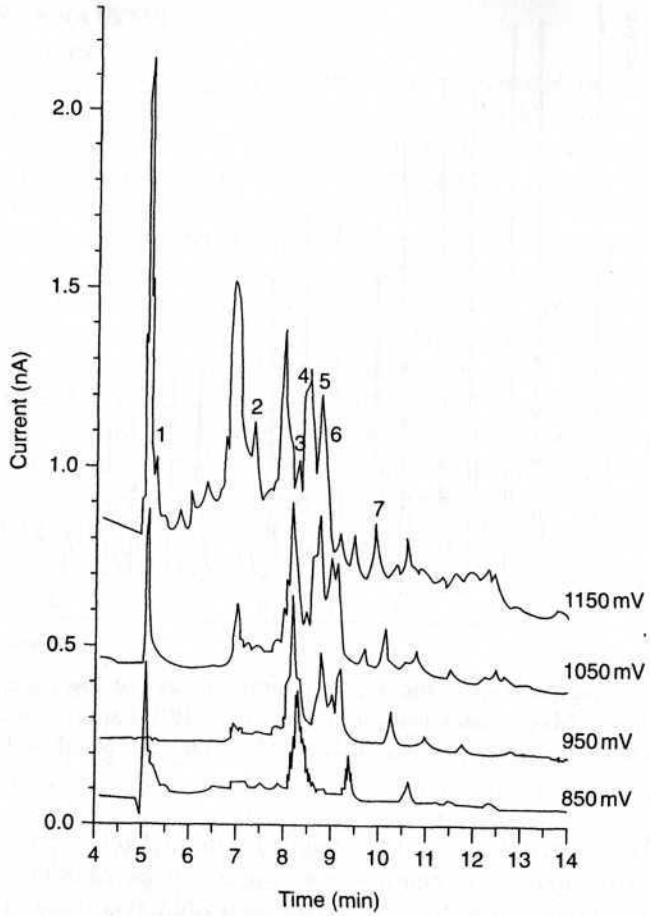

Figure 3.24 Capillary electrophoresis/amperometric response of a Bud Light beer sample using different detection potentials. (Reproduced with permission from Ref. 72.)

troactive functionalities) and for improving the detection of species with normally unfavorable redox properties. Post-column addition can also be used to adjust the conditions (e.g., pH) to meet the needs of the electrochemical detection.

3.6.2 Cell Design

A wide range of cell designs have been used for electrochemical monitoring of flowing streams. The cell design must fulfill the requirements of high signal : noise ratio, low dead volume, well-defined hydrodynamics, small ohmic drop, and ease of construction and maintenance (polishing). In addition, the reference and counter electrodes should be located on the downstream side of the working electrode, so that reaction products at the counter electrode or leakage from the reference electrode do not interfere with the working electrode. The distance between the column outlet and the working electrode affects the post-separation band broadening.

The most widely used amperometric detectors are based on the thin-layer and wall-jet configurations (Fig. 3.25). The thin-layer cell relies on a thin layer of solution that flows parallel to the planar electrode surface, which is embedded in a rectangular channel. The flow channel is formed by two plastic blocks pressing a thin Teflon gasket, which defines the very small dead volume (~1 μL). In the wall-jet design, the stream flows from a nozzle perpendicularly onto a flat electrode surface (the wall), and then spreads radially over the surface. The electrode diameter is significantly larger than the nozzle inlet. Since the jet remains intact up to quite large inlet electrode separations, it is possible to employ also large-volume wall-jet detectors that offer decreased sensitivity to the properties of the mobile phase, and a simplified fabrication. Both the thin-layer and wall-jet designs commonly rely on disk working electrodes made of carbon (e.g., glassy carbon, diamond, or paste) or metal (such as gold or platinum).

It is also possible to employ detectors with solutions flowing over a static mercury drop electrode or a carbon fiber microelectrode, or to use flow-through electrodes, with the electrode simply an open tube or porous matrix. The latter can offer complete electrolysis, namely, coulometric detection. The extremely small dimensions of ultramicroelectrodes (discussed in Section 4.5.4) offer the advantages of flow-rate independence (and hence a low noise level) and operation in nonconductive mobile phases (such as those of normal-phase chromatography or supercritical fluid chromatography).

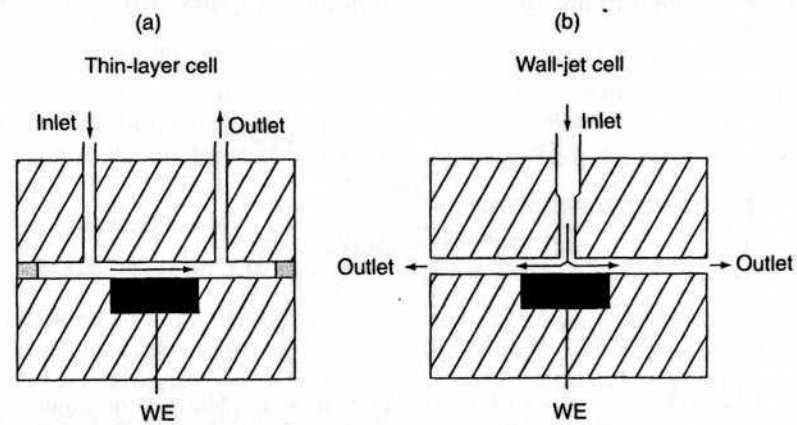

Figure 3.25 Common detector configurations: thin-layer (channel) (a) and wall-jet (b) flow cells.

Ultramicroelectrodes can also greatly benefit modern microseparation techniques such as open-tube liquid chromatography or capillary-zone electrophoresis (CZE) (73). For example, cylinder-shaped carbon or copper fibers can be inserted into the end of the CE separation capillary (e.g., see Fig. 3.26). Such alignment of the working electrode with the end of the capillary represents a challenge in combining electrochemistry with CZE.

Capillary-zone electrophoresis has more recently established itself as an important separation tool, due to its impressive separation power. Since CZE separations rely on the application of strong electric fields for separating the analytes, it is essential to isolate the low detection potential from the high voltage (10–30 kV) used to effect the separation (75). This can be accomplished by using a decoupling device (e.g., Nafion or cellulose acetate joints, porous glass) or via an end-column detection (i.e., placement of the detector opposite to the capillary outlet). The latter relies on the dramatic drop of the potential across small capillaries (of ≤25 μm). Figure 3.27 depicts a typical end-column electropherogram for femtomole quantities of dopamine, isoproterenol, and catechol. Since the sensitivity of electrochemical detection is not compromised by the low volumes used in CZE systems, extremely low mass detection limits (in the attomole range) can be obtained. Such high sensitivity toward easily oxidizable or reducible analytes rivals that of laser-induced fluorescence [which is currently (as of 2005) the method of choice for most CZE applications], and makes CZE/electrochemistry an ideal tool for assays of many small-volume samples.

Electrochemical detection offers also great promise for CZE microchips, and for other chip-based analytical microsystems (e.g., "Lab-on-a-Chip) discussed in Section 6.3 (77–83). Particularly attractive for such microfluidic devices are the high sensitivity of electrochemical detection, its inherent miniaturization of both the detector and control instrumentation, low cost, low power demands, and compatibility with micromachining technologies. Various detector configurations, based on different capillary/working-electrode

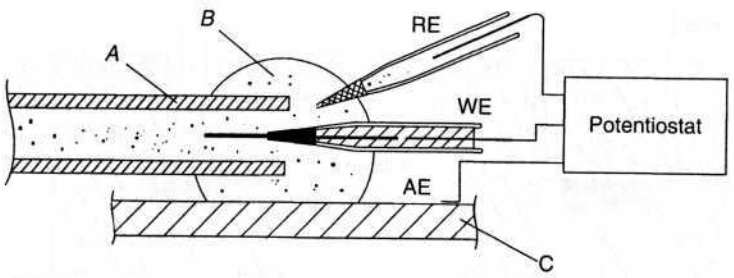

Figure 3.26 Schematic of a carbon fiber amperometric detector for capillary electrophoresis: *A*, fused-silica capillary; *B*, eluent drop; *C*, stainless-steel plate; RE, reference electrode; WE, working electrode, AE, auxiliary electrode. (Reproduced with permission from Ref. 74.)

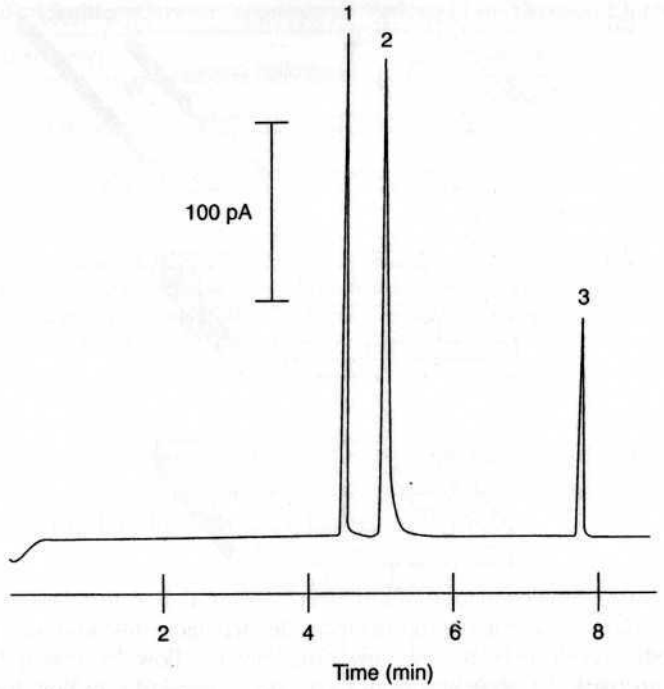

Figure 3.27 Electrophoretic separation of catechols with an end-column detection. Detection potential, +0.8 V; separation voltage, 20 kV. The peaks correspond to 4.6 fmol dopamine (1), 4.1 fmol isoproterenol (2), and 2.7 fmol catechol (3). (Reproduced with permission from Ref. 76.)

arrangements and the position of the electrode relative to the flow direction, have been proposed. These include flow-by (80), flow-onto (81), and flow-through (82) configurations (Fig. 3.28). In-channel detection (i.e., placement of a flow-by working electrode within the separation channel), which obviates postcapillary band dispersion effects, is also possible but usually requires an electrical decoupler that isolates the detector from the separation voltage (83).

3.6.3 Mass Transport and Current Response

Well-defined hydrodynamic conditions, with high rate of mass transport, are essential for a successful use of electrochemical detectors. According to the Nernst approximate approach, the thickness of the diffusion layer (δ) is empirically related to the solution flow rate (U) via

$$\delta = B/U^{\alpha} \tag{3.32}$$

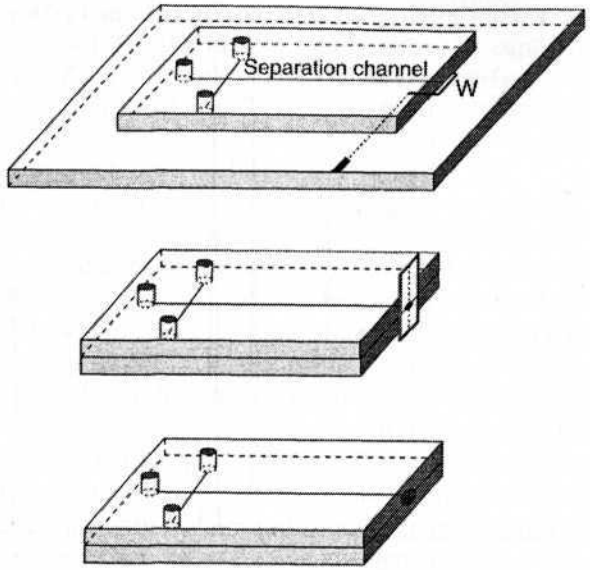

Figure 3.28 Common configurations of electrochemical detectors for CE microchips, based on different capillary/working-electrode arrangements and the position of the electrode (w) relative to the flow direction: (a) flow by (using two plates); (b) flow onto (with the surface normal to the flow direction); (c) flow through (with the detector placed directly on the channel exit). (Reproduced with permission from Ref. 78.)

where B and α are constants for a given set of conditions, with α ranging between 0.33 and 1.0. By substituting Eq. (3.32) in the general current response for mass-transport-controlled reactions [$i_l = (nFADC/\delta)$], one obtains the limiting steady-state response of flow-through electrodes

$$i_l = nFAK_m CU^{\alpha} \tag{3.33}$$

where K_m is the mass transport coefficient (D/B).

A more rigorous treatment takes into account the hydrodynamic characteristics of the flowing solution. Hence, expressions for the limiting currents (under steady-state conditions) have been derived for various electrode geometries by solving the three-dimensional convective diffusion equation:

$$\frac{\partial C}{\partial t} = D\left(\frac{\partial^2 C}{\partial x^2} + \frac{\partial^2 C}{\partial y^2} + \frac{\partial^2 C}{\partial z^2}\right) - \left(U_x \frac{\partial C}{\partial x} + U_y \frac{\partial C}{\partial y} + U_z \frac{\partial C}{\partial z}\right) \tag{3.34}$$

The resulting equations, arrived at by setting appropriate initial and boundary conditions (depending on the particular electrode), are given in Table 3.4.

TABLE 3.4 Limiting-Current Response of Various Flow-Through Electrodes[a]

Electrode Geometry	Limiting-Current Equation
Tubular	$i = 1.61nFC(DA/r)^{2/3}U^{1/3}$
Planar (parallel flow)	$i = 0.68nFCD^{2/3}\nu^{-1/6}(A/b)^{1/2}U^{1/2}$
Thin-layer cell	$i = 1.47nFC(DA/b)^{2/3}U^{1/3}$
Planar (perpendicular)	$i = 0.903nFCD^{2/3}\nu^{-1/6}A^{3/4}u^{1/2}$
Wall-jet detector	$i = 0.898nFCD^{2/3}\nu^{-5/12}a^{-1/2}A^{3/8}U^{3/4}$

[a] *Definition of terms*: a = diameter of inlet, A = electrode area, b = channel height, C = concentration (mM), F = Faraday constant, D = diffusion coefficient, ν = kinematic viscosity, r = radius of tubular electrode, U = average volume flow rate, u = velocity (cm/s), n = number of electrons. *Source*: Adapted from Ref. 84.

A generalized equation for the limiting current response of different detectors, based on the dimensionless Reynolds (Re) and Schmidt (Sc) numbers, has been derived by Hanekamp and coworkers (84)

$$i_l = nkFCD(\mathrm{Sc})^{\beta} b(\mathrm{Re})^{\alpha} \tag{3.35}$$

where k is a dimensionless constant and b is the characteristic electrode width.

In the case of coulometric detectors (with complete electrolysis), the limiting current is given by Faraday's law:

$$i_l = nFCU \tag{3.36}$$

3.6.4 Detection Modes

The simplest, and by far the most common, detection scheme is measurement of the current at a constant potential. Such fixed-potential amperometric measurements have the advantage of being free of double-layer charging and surface transient effects. As a result, extremely low detection limits—on the order of 1–100 pg (~10^{-14} mol of analyte)—can be achieved. In various situations, however, it may be desirable to change (scan, pulse, etc.) the potential during the detection.

Potential-scanning detectors can increase the information content over that of fixed-potential operation. By rapidly recording numerous voltammograms during the elution, one obtains a three-dimensional detector response of the current against potential and time. Such addition of the redox potential selectivity can offer immediate identification of eluting peaks, and helps resolve chronomatographically coeluting components. Different approaches to swept-potential detectors based on square-wave voltammetry (14,15), frequency-based sinusoidal voltammetry (21), or phase-sensitive AC voltammetry (85) have been reported. The greater selectivity of potential-scanning detection is

accompanied by higher detection limits (vs. fixed-potential amperometry), because of the additional background current associated with the potential scan.

Pulsed amperometric detection (PAD), introduced by Johnson and LaCourse (86,87) has greatly enhanced the scope of liquid chromatography/electrochemistry (88). This detection mode overcomes the problem of lost activity of noble metal electrodes associated with the fixed-potential detection of compounds such as carbohydrates, alcohols, amino acids, or aldehydes. Pulsed amperometric detection couples the process of anodic detection with anodic cleaning and cathodic reactivation of a noble-metal electrode, thus assuring a continuously cleaned and active surface. This is usually accomplished with a three-step potential waveform, combining anodic and cathodic polarizations (e.g., see Fig. 3.29). The analytical response results primarily from adsorbed analyte, with detection limits approaching 50 ng (for 50-μL samples). Other automated multistep potential waveforms are possible. Such waveforms are commonly executed at a frequency of 1–2 Hz, in connection with gold or platinum working electrodes.

The power of electrochemical detection can be improved by using more than one working electrode (89). Different strategies, based primarily on dual-electrode detection, can thus be employed. For example, in the series mode (Fig. 3.30, top) the first upstream electrode can be used to generate an electroactive species that is then more easily detected at the downstream electrode. Discrimination against compounds with irreversible redox chemistry can also be achieved. Significantly improved qualitative information can be

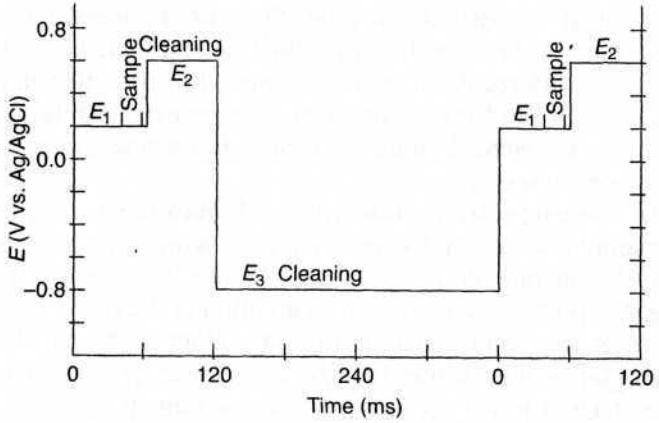

Figure 3.29 Triple-pulse amperometric waveform.

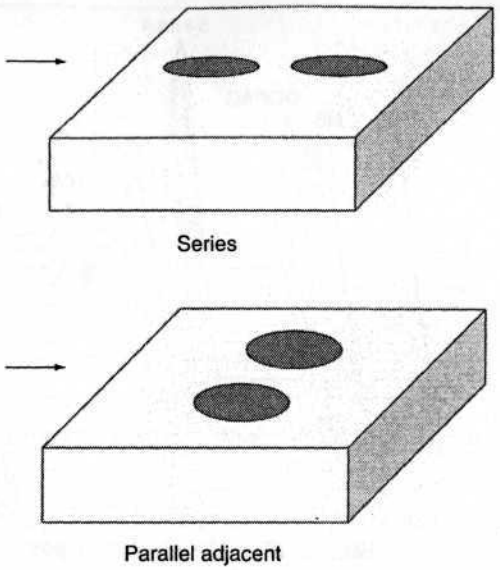

Figure 3.30 Dual-electrode thin-layer detector configurations for operation in the series (top) and parallel (bottom) amperometric modes.

achieved using a parallel (side-by-side) dual-electrode configuration (Fig. 3.30, bottom). Two simultaneous chromatograms can be generated by holding these electrodes at different potentials. The current ratios at these two potential settings provide real-time "fingerprints" of the eluting peaks. Such ratio values are compared with those of standards to confirm the peak identity. Further improvements in the information content can be achieved using multichannel amperometric detection (analogous to diode array optical detection) (90). For example, Figure 3.31 displays a three-dimensional chromatogram for a mixture of several biologically significant compounds at a 16-electrode detector array. By rapidly applying a five-potential sequence to the individual electrodes, an 80-channel chromatographic detection can be obtained. Such an electrochemical profile across the array provides confirmation of peak purity and improved identification of target analytes. Additional information can be obtained by using arrays comprised of different electrode materials (see Section 6.4). For a more detailed description of on-line electrochemical detectors, the reader is referred to a monograph by Stulik and Pacáková (91). Comparison of various commercial detectors is also available (92).

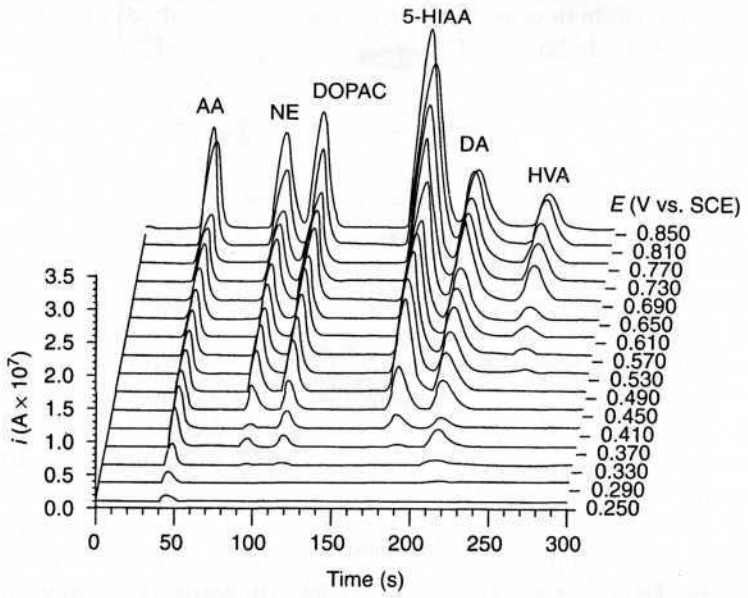

Figure 3.31 Three-dimensional chromatogram for oxidizable biological compounds at a multichannel amperometric detection system, consisting of an array of 16 carbon paste electrodes poised at different potentials. (Reproduced with permission from Ref. 90.)

EXAMPLES

Example 3.1 Voltammogram *a* was obtained for adsorptive stripping measurements of Fe(III) in seawater. Voltammograms *b* and *c* show successive standard additions of 4 ppb Fe(III). Find the concentration of Fe(III) in the sample.

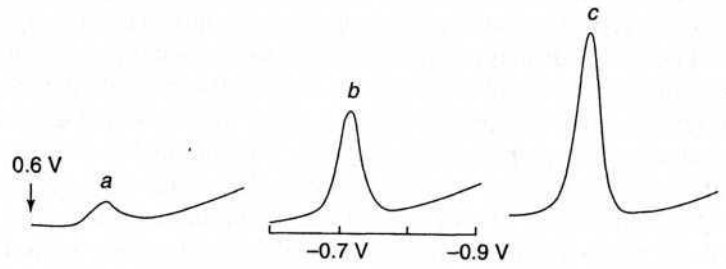

Solution The resulting current peaks lead to the following standard addition plot:

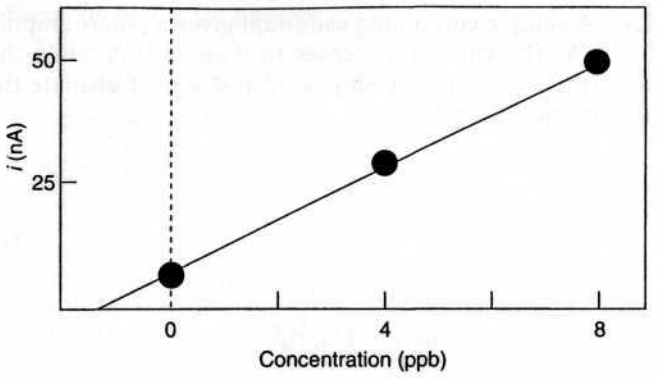

From this plot, an Fe(III) concentration of 1.47 ppb can be obtained for the sample.

Example 3.2 Calculate the limiting current that would be expected from the reduction of 2×10^{-4} M Pb^{2+}, using the DME characteristics, $m = 2.0$ mg/s and $t = 4$ s. The diffusion coefficient of Pb^{2+} is 1.01×10^{-5} cm^2/s.

Solution The lead reduction is a two-reduction process:

$$Pb^{2+} + 2e^- \rightleftharpoons Pb$$

Hence, from the Ilkovic equation, (2.4), we obtain

$$I_d = 708 \times 2 \times (1.01 \times 10^{-5})^{1/2} (2.0)^{2/3} \times 4^{1/6} \times 0.2 = 1.81\,\mu A$$

Example 3.3 Draw the DC polarographic response for a mixture containing 3 mM Cu^{2+}, 2 mM Zn^{2+}, and 1 mM Cd^{2+}. The half-wave potentials for the Cu, Zn, and Cd ions are −0.12, −0.95, and −0.62 V, respectively.

Solution

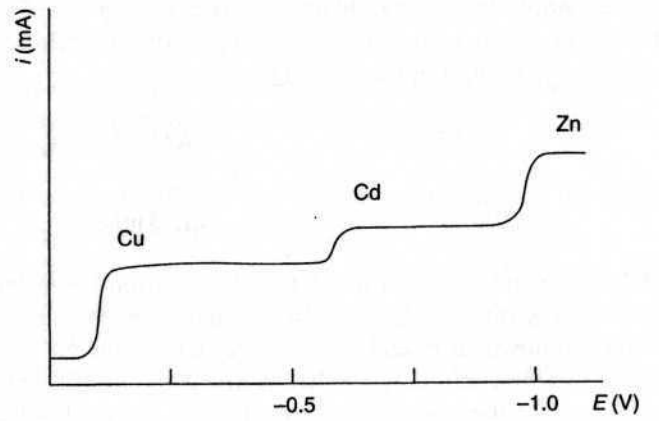

Example 3.4 A sample containing cadmium gives a polarographic reduction current of 6.0 μA. The current increases to 9 and 12 μA when the cadmium concentration is increased in two steps of 2 mM each. Calculate the cadmium concentration in the original sample.

Solution

$$6 = KC$$
$$9 = K(C+2)$$
$$12 = K(C+4)$$

to yield a C value of 4 mM.

Example 3.5 Polarogram *a* was obtained for a 10-mL lead-containing sample. The limiting current increased (to B) after addition of 100 μL of a 0.10-M lead standard to the 10-mL sample. Calculate the original lead concentration in the sample.

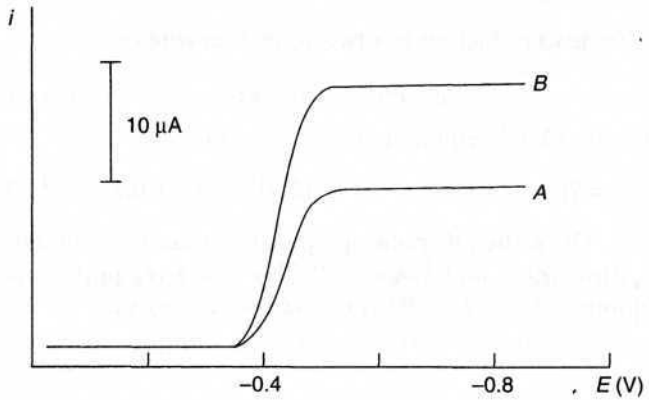

Solution The sample lead ion yielded a limiting current of 13 μA (A). The current increases by 8.5 μA on spiking the sample with a 1-mM lead standard (considering the 1 : 100 fold dilution; B-A).

$$i_l = KC \qquad 8.5 = K(1\,\text{mM})$$
$$K = 8.5$$
$$13.0 = 8.5C_{\text{sample}} \qquad C_{\text{sample}} = 1.53\,\text{mM}$$

Example 3.6 Flow analysis of a urine sample at a thin-layer amperometric detector, with a flow-rate of 1.25 mL/min, yielded a limiting current value of 1.6 μA for its unknown uric acid content. A larger current of 2.4 μA was observed for a sample containing 1×10^{-4} M uric acid and flowing at a rate of 0.9 mL/min. Calculate the original concentration of uric acid in the sample.

Solution From Table 3.4, we obtain

$$i_l = KCU^{1/3}$$
$$2.4 = K(1\times10^{-4})0.9^{1/3} \qquad K = 2.49\times10^4$$
$$1.6 = 2.49\times10^4(C)1.25^{1/3} \qquad C = 6\times10^{-5}\,\text{M}$$

PROBLEMS

3.1 Describe the principle and operation of potentiometric stripping analysis (PSA). How does it differ from anodic stripping voltammetry (ASV)? What is the quantitative signal? What, if any, are its advantages over ASV?

3.2 Draw schematic diagrams of a thin-layer flow detector utilizing an (a) single working electrode and (b) a dual electrode. Explain how the latter improves the power and information content.

3.3 The detection of nitroaromatic explosives in seawater requires a fast (1-s) and sensitive response (down to the 10 nM level). Discuss an electrochemical technique most suitable for such assays and the optimization of its variables for achieving this important goal. Clarify your choice. What is the basis for the observed response? What are the potential interferences?

3.4 Describe and draw the waveform employed in square-wave voltammetry. Explain how the current is being measured.

3.5 Why is it essential to wait ~40 ms after the potential step in normal pulse polarography before sampling the current?

3.6 Describe the use of polarographic analysis for obtaining the values of the formation constant and stoichiometric number of metal complexes.

3.7 Describe the challenges of interfacing electrochemical detectors to capillary electrophoresis separation systems. How can these challenges be addressed?

3.8 Explain how and why the coupling of stripping voltammetry to a differential-pulse waveform can enhance the power of stripping measurements of trace metals.

3.9 Select an electrochemical technique most suitable for detecting trace levels of nickel in groundwater. Explain your choice.

3.10 A liquid chromatographic experiment resulted in the same retention time for the electroactive compounds A and B ($E°$A = +0.43 V; $E°$ B = +0.77 V). Which electrochemical detection scheme would offer a selective detection of the two coeluting analytes? Explain your selection.

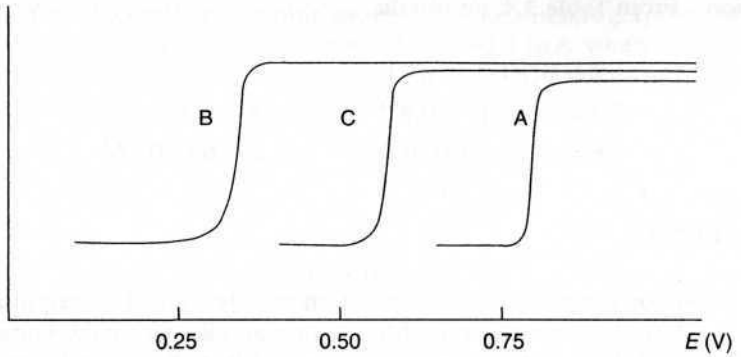

3.11 Use the adsorption theory (of Section 2.1.3) to explain why adsorptive stripping voltammetry results in nonlinear calibration plots.

3.12 Derive the Cottrell equation by combining Fick's first law of diffusion with the time-dependent change of the concentration gradient during a potential step experiment.

3.13 The oxidizable compounds A, B, and C display the following hydrodynamic voltammograms:

Determine which operating potential will allow (a) selective flow injection detection of B in the presence of A and C and (b). selective HPLC measurements of A ($t_{r,A} = 18$ min; $t_{r,B} = 18$ min, $t_{r,C} = 11$ min); explain your choices.

3.14 While carbohydrates and alcohols can be oxidized at gold electrodes, they cannot be detected by fixed-potential amperometry. Explain why, and suggest an alternative more suitable detection scheme for their measurements in flowing streams.

REFERENCES

1. Ilkovic, D., *Coll. Czech. Chem. Commun.* **64**, 498 (1934).
2. Lingane, J., *Chem. Rev.* **29**, 1 (1941).
3. Barker, G. C.; Jenkin, I. L., *Analyst* **77**, 685 (1952).
4. Barker, G. C.; Gardner, A. W., *Z. Anal. Chem.* **173**, 79 (1960).
5. Osteryoung, J.; Kirowa-Eisner, E., *Anal. Chem.* **52**, 62 (1980).
6. Parry, E. P.; Osteryoung, R. A., *Anal. Chem.* **37**, 1634 (1964).
7. Flato, J. B., *Anal. Chem.* **44**, 75A (1972).
8. Osteryoung, J.; Osteryoung, R. A., *Anal. Chem.* **57**, 101A (1985).
9. O'Dea, J. J.; Osteryoung, J.; Osteryoung, R. A., *Anal. Chem.* **53**, 695 (1981).
10. Borman, S., *Anal. Chem.* **54**, 698A (1982).
11. Wang, J.; Lu, F.; MacDonald, D.; Lu, J.; Ozsoz, M.; Rogers, K., *Talanta* **46**, 1405 (1998).
12. Yarnitzky, C., *Anal. Chem.* 57, 2011 (1985).
13. Wang, J.; Ouziel, E.; Yarnitzky, C.; Ariel, M., *Anal. Chim. Acta* **102**, 99 (1978).

14. Samuelsson, R.; O'Dea, J. J.; Osteryoung, J., *Anal. Chem.* **52**, 2215 (1980).
15. Gerhardt, G. C.; Cassidy, R. M.; Baranski, A. S., *Anal. Chem.* **70**, 2167 (1998).
16. Stefani, S.; Seeber, R., *Anal. Chem.* **54**, 2524 (1982).
17. Breyer, B.; Bauer, H., *Rev. Polarogr.* **8**, 157 (1960).
18. Smith, D. E., *CRC Crit. Rev. Anal. Chem.* **2**, 247 (1971).
19. Breyer, B.; Bauer, H., *Alternating Current Polarography and Tensammetry*, Wiley-Interscience, New York, 1963.
20. Brazill, S. A.; Bender, S. E.; Hebert, N. E.; Cullison, J. K.; Kristensen, E. W.; Kuhr, W. G., *J. Electroanal. Chem.* **531**, 119 (2002).
21. Hebert, N.; Kuhr, W.; Brazill, S., *Anal. Chem.* **75**, 3301 (2003).
22. Zhang, J.; Guo, S.; Bond, A. M.; Marken, F., *Anal. Chem.* **76**, 3619 (2004).
23. Wang, J., *Stripping Analysis: Principles, Instrumentation and Applications*, VCH Publishers, Deerfield Beach, FL, 1985.
24. Copeland, T. R.; Skogerboe, R. K., *Anal. Chem.* **46**, 1257A (1974).
25. Florence, T. M., *J. Electroanal. Chem.* **27**, 273 (1970).
26. Economou, A.; Fielden, P. R., *Analyst* **128**, 205 (2003).
27. Wang, J.; Lu, J.; Hocevar, S.; Farias, P.; Ogorevc, B., *Anal. Chem.* **72**, 3218 (2000).
28. Wang, J., *Electroanalysis* **17**, 1341 (2005).
29. Marken, F.; Rebbitt, T. O.; Booth, J.; Compton, R. G., *Electroanalysis* **9**, 19 (1997).
30. Jagner, D., *Trends. Anal. Chem.* **2**(3), 53 (1983).
31. Wang, J., "Voltammetry after nonelectrolytic proconcentration," in A. J. Bard, ed., *Electroanalytical Chemistry*, Marcel Dekker, New York, 1989, Vol. 16, p. 1.
32. Van den Berg, C. M. G., *Anal. Chim. Acta* **250**, 265 (1991).
33. Paneli, M.; Voulgaropoulos, A., *Electroanalysis* **5**, 355 (1993).
34 Van den Berg, C. M. G.; Murphy, K.; Riley, J. P., *Anal. Chim. Acta* **188**, 177 (1986).
35. Wang, J.; Baomin, T., *Anal. Chim. Acta* **270**, 137 (1992).
36. Donat, J. R.; Bruland, K. W., *Anal. Chem.* **60**, 240 (1988).
37. Golimowski, J.; Valenta, P.; Nürnberg, H. W., *Fres. Z. Anal. Chem.* **322**, 315(1985).
38. Wang, J.; Mahmoud, J. S., *Fres. Z. Anal. Chem.* **327**, 789 (1987).
39. Wang, J.; Mahmoud, J. S., *J. Electroanal. Chem.* **208**, 383 (1986).
40. van den Berg, C. M. C., *Anal. Chem.* **57**, 1532 (1985).
41. Pihlar, B.; Valenta, P.; Nürnberg, H. W., *Fres. Z. Anal. Chem.* **307**, 337 (1981).
42. Wang, J.; Zadeii, J.; Lin, M. S., *J. Electroanal. Chem.* **237**, 281 (1987).
43. Wang, J.; Zadeii, J., *Talanta* **34**, 909 (1987).
44. Yokoi, K.; van den Berg, C. M. C., *Anal. Chim. Acta* **245**, 167 (1991).
45. Van den Berg, C. M. G.; Nimmo, N., *Anal. Chem.* **59**, 269 (1987).
46. Van den Berg, C. M. G., *Anal. Chem.* **56**, 2383 (1984).
47. Wang, J.; Cai, X.; Jonsson, C.; Balakrishan, M., *Electroanalysis* **8**, 20 (1996).
48. Luther, G. W.; Swartz, C.; Ullman, W., *Anal. Chem.* **60**, 1721 (1988).
49. Scholz, F.; Lange, B., *Trends Anal. Chem.* **11**, 359 (1992).
50. Tercier, M.; Buffle, J., *Electroanalysis* **5**, 187 (1993).
51. Komanur, N. K.; van Loon, G. W., *Talanta* **24**, 184 (1977).
52. Poldoski, J.; Glass, G., *Anal. Chim. Acta* **101**, 79 (1978).

53. Wang, J.; Lu, J.; Olsen, K., *Analyst* **117**, 1913 (1992).
54. Hutton, E.; van Elteren, J.; Ogorevc, B.; Smyth, M., *Talanta* **63**, 849 (2004).
55. Gottesfeld, S.; Ariel, M., *J. Electroanal. Chem.* **9**, 112 (1965).
56. Wang, J.; Mannino, S., *Analyst* **114**, 643 (1989).
57. Obata, H.; van den Berg C. M. C., *Anal. Chem.* **73**, 2522 (2001).
58. Ostapczuk, P., *Clin. Chem.* **38**, 1995 (1992).
59. Lai, P.; Fung, K., *Analyst* **103**, 1244 (1978).
60. Golimowski, J.; Gustavsson, I., *Fres. Z. Anal. Chem.* **317**, 484 (1984).
61. Adeloju, S. B.; Bond, A. M.; Briggs, M. H., *Anal. Chim. Acta* **164**, 181 (1984).
62. Hoppstock, K.; Michulitz, M., *Anal. Chim. Acta* **350**, 135 (1997).
63. Porbes, S.; Bound, G.; West, T., *Talanta* **26**, 473 (1979).
64. Levit, D. I., *Anal. Chem.* **45**, 1291 (1973).
65. Wang, J.; Setiadji, R.; Chen, L.; Lu, J.; Morton, S., *Electroanalysis* **4**, 161 (1992).
66. Williams, T.; Foy, O.; Benson, C., *Anal. Chim. Acta* **75**, 250 (1975).
67. Cavicchioli, A.; La-Scalea, M. A.; Gutz, I. G., *Electroanalysis* **16**, 697 (2004).
68. Florence, T. M., *Analyst* **111**, 489 (1986).
69. Wang, J., *Analyst* **119**, 763 (1994).
70. Tercier, M. L.; Buffle, J.; Graziottin, F., *Electroanalysis* **10**, 355 (1998).
71. Wang, J., *Anal. Chim. Acta* **500**, 247 (2003).
72. Moane, S.; Park, S.; Lunte, C. E.; Smyth, M. R., *Analyst* **123**, 1931 (1998).
73. Ewing, A. G.; Mesaros, J. M.; Gavin, P. F., *Anal. Chem.* **66**, 527A (1994).
74. Curry, P.; Engstrom, C.; Ewing, A., *Electroanalysis*, **3**, 587 (1991).
75. Holland, L. A.; Lunte, S. M., *Anal. Commun.* **35**, 1H (1998).
76. Sloss, S.; Ewing, A. G., *Anal. Chem.* **63**, 577 (1993).
77. Woolley, A.; Lao, K.; Glazer, A.; Mathies, R., *Anal. Chem.* **70**, 684 (1998).
78. Wang, J., *Electroanalysis* **17**, 1133 (2005).
79. Lacher, N. A.; Garrison, K. E.; Martin, R. S.; Lunte, S. M., *Electrophoresis* **22**, 2526 (2001).
80. Woolley, T.; Lao, K.; Glazer, A. N.; Mathies, R. A., *Anal. Chem.* **70**, 684 (1998).
81. Wang, J.; Tian, B.; Sahlin, E., *Anal. Chem.* **71**, 5436 (1999).
82. Hilmi, A.; Luong, J. H., *Anal. Chem.* **72**, 4677 (2000).
83. Chen, D.; Hsu, F.; Zhan, D.; Chen, C., *Anal. Chem.* **73**, 758 (2001).
84. Hanekamp, H. B.; Box, P.; Frei, R. W., *Trends Anal. Chem.* **1**, 135 (1982).
85. Trojanek, A.; De Jong, H. G., *Anal. Chim. Acta* **141**, 115 (1982).
86. Johnson, D. C.; LaCourse, W. R., *Anal. Chem.* **62**, 589A (1990).
87. Johnson, D.C.; LaCourse, W. R., *Electroanalysis* **4**, 367 (1992).
88. LaCourse, W. R., *Pulsed Electrochemical Detection in HPLC*, Wiley, New York, 1997.
89. Roston, D. A.; Shoup, R. E.; Kissinger, P. T., *Anal. Chem.* **54**, 1417A (1982).
90. Hoogvliet, J.; Reijn, J.; van Bennekom, W., *Anal. Chem.* **63**, 2418 (1991).
91. Stulik, K.; Pacáková, V., *Electroanalytical Measurements in Flowing Liquids*, Ellis Horwood, Chichester, UK, 1987.
92. Warner, M., *Anal. Chem.* **66**, 601A (1994).

4

PRACTICAL CONSIDERATIONS

The basic instrumentation required for controlled-potential experiments is relatively inexpensive and readily available commercially. The basic necessities include a cell (with a three-electrode system), a voltammetric analyzer (consisting of a potentiostatic circuitry and a voltage ramp generator), and a plotter. Modern voltammetric analyzers are versatile enough to perform many modes of operation. Depending on the specific experiment, other components may be required. For example, a faradaic cage is desired for work with ultramicroelectrodes. The system should be located in a room free from major electrical interferences, vibrations, and drastic fluctuations in temperature.

4.1 ELECTROCHEMICAL CELLS

Three-electrode cells (e.g., see Fig. 4.1) are commonly used in controlled-potential experiments. The cell is usually a covered beaker of 5–50 mL volume, and contains the three electrodes (working, reference, and auxiliary), which are immersed in the sample solution. While the working electrode is the electrode at which the reaction of interest occurs, the reference electrode provides a stable and reproducible potential (independent of the sample composition), against which the potential of the working electrode is compared. Such "buffering" against potential changes is achieved by a constant composition of both forms of its redox couple, such as Ag/AgCl or Hg/Hg_2Cl_2, as common

Analytical Electrochemistry, Third Edition, by Joseph Wang